The Pennsylvania State University

The Graduate School

Department of Material Science and Engineering

MEASURING HYDRATION OF CATIONIC POLYMERS USING AZIDE AS A PROBE

A Thesis in

Material Science and Engineering

by

Raymond Lopez-Hallman

Submitted in Partial Fulfillment
of the Requirements
for the Degree of

Master of Science

August 2017

The thesis of Raymond Lopez-Hallman was reviewed and approved* by the following:

Michael A. Hickner
Associate Professor of Materials Science and Engineering
Thesis Advisor

James Runt
Professor of Polymer Science

Robert Hickey
Assistant Professor of Material Science and Engineering

Suzanne Mohney
Professor of Materials Science and Engineering
Chair, Intercollege Graduate Degree Program in Materials Science and Engineering

*Signatures are on file in the Graduate School

ABSTRACT

As clean alternative energy conversion devices, fuel cells using proton exchange membranes (PEM) are a promising technology. However, high-cost noble-metal catalysts (typically platinum) hinder their widespread commercialization. Anion exchange membrane (AEM) fuel cells employ cationic moieties tethered to polymer chains and do not require expensive noble-metal catalysts due to their high internal device pH. Thus, AEMs are considered a next generation of fuel cells for stationary and transportation applications. To date, AEMs have their own set of challenges that need to be understood, including inferior conductivity and stability compared to PEMs. Water interactions within the cationic polymer membranes remain unexplored and are important for understanding and improving the ion conductivity of these materials. The main goal of thesis was to measure the hydration of cationic polymers with Fourier transform infrared (FTIR) spectroscopy using the azide anion as a vibrational probe. Using azide (N_3^-) as a probe has the advantage of being a small molecule, is soluble in water, and has a strong IR absorption band.

With the objective of understanding hydration in AEMs, this thesis work was subdivided into two parts. The first part of the work focused on understanding the interaction of the azide (as $TBAN_3$) in different solvent mixture environments as a foundation for its use as a vibrational probe. Studies were conducted on four sets of mixtures: dimethyl sulfoxide (DMSO)-H_2O, tetrahydrofuran (THF)-H_2O, chloroform-methanol (MeOH), and DMSO-chloroform. The FTIR spectra for these four sets of mixtures were analyzed, fitted using the appropriate number of mixed

Lorentzian/Gaussian functions, and used to interpret the polymer spectra. Overall, it was observed that hydrogen bonding played a more dominant role for the peak position of the azide asymmetric stretch band, rather than the dielectric constant of the solvents and mixtures. The azide asymmetric stretch band blueshifted to a higher frequency contingent on each solvent's ability to form hydrogen bonds with the azide. Based on these findings, polar protic solvents, such as H_2O and MeOH, which are strong hydrogen bond donors, were able to interact strongly with the azide, which is a hydrogen bond acceptor. Also, the polar aprotic solvents, such as DMSO and THF, interacted weakly with the azide. Interestingly, chloroform showed an intermediate interaction because of its ability to form a bifurcated hydrogen bond with the azide.

The second part of the work focused on studying a series of quaternary ammonium containing poly(2,6-dimethyl-1,4-phenylene oxide) (QA-PPO) cationic polymers, as a model of an AEM experimental system, to measure their hydration behavior. Three comb-shaped QA-PPO polymers were synthesized with a pendant n-alkyl side chain of six, ten and sixteen carbons; respectively, benzyldimethylhexyl ammonium, benzyldimethyldecyl ammonium, and benzyldimethylcetyl ammonium; or C6, C10, and C16, in short. A control polymer was also synthesized with the same degree of bromination (0.4 bromomethyl groups per PPO repeat unit) but without a pendant alkyl side chain, referred to as benzyltrimethyl ammonium (BTMA). Thin films of the QA-PPO polymer samples were saturated with sodium azide (NaN_3) and measured in-situ by attenuated total reflectance (ATR) FTIR, during hydration from 0 to 90% relative humidity (RH). All RH data was calculated to their respected hydration number (λ), taking into consideration their ionic exchange capacity (IEC). All recorded FTIR spectra

of the azide asymmetric stretch bands for the different QA-PPOs were presented, with the frequency of the azide band expressed as a function of λ. QA-PPO BTMA, C6, C10, and C16 had different interactions with the azide and sodium azide species as evidenced by the position and intensity of their characteristic FTIR bands. For BTMA the wavenumber of the azide group was at ~2000 cm^{-1} and 2026 cm^{-1} at 0% RH (λ=0) and 90% RH (λ=4.3), respectively. For C16, the azide absorbance band was observed at approximately 2000 cm^{-1} and 2020 cm^{-1} at 0% RH and 90% RH, respectively. The frequency of the azide band for the other comb-shaped polymers (C6 and C10) fell in-between the two parameters discussed above.

Overall, these results indicate that the interaction of the QA-PPOs with water becomes stronger as the alkyl pendant becomes shorter; as evidenced by the observation that BTMA had more bulk-like water values at each λ (or % RH), and possibly indicative of higher water mobility within BTMA than within the comb-shaped polymers. When the fitted spectra data for BTMA and C16 (representing the two limits) at their respective RH was presented, the results better illustrated the behavior of the QA-PPOs. With the dry samples, the bands for the "free" azides (at 2000 cm^{-1}) were most prominent; but with increasing λ, the bands for the "free" azides and the azides interacting with the QA groups (at ~2007 cm^{-1}) decreased while the azides interacting with water increased. Upon comparison between BTMA and C16, it was noted that for C16 a higher hydration level (>25% RH) was required to eliminate the "free" azide band. It is assumed that the presence of alkyl side chains in C16 made it more difficult for the mobility of the water molecules within the membrane, and to promptly access all "free" azides in the system.

In conclusion, the azide anion was successfully employed as a vibrational probe to measure the changes in water and polymer interactions and was effectively measured by ATR-FTIR. Further expansion of research in this area will lead to a better understanding of the ionic transportation and conductivity properties of cationic polymer membranes, such as the QA-PPOs. Understanding these properties is one of many steps needed to be taken in order to improve AEM technology and develop useful applications, such as energy and water purification systems.

TABLE OF CONTENTS

LIST OF ABBREVIATION

FCTO = Fuel Cell Technologies Office

PEFC = polymer electrolyte fuel cell

AFC = alkaline fuel cell

GDL = gas diffusion layer

ECL = electroactive catalystic layer

GDE = gas diffusion electrode

HOR = hydrogen oxidation reaction

ORR = oxygen reduction reaction

PAFC = phosphoric acid fuel cell

AEM = anion exchange membranes

PEM = proton exchange membrane

AAEM = alkaline anion exchange membrane

PGM = platinum group metal

PFSA = perfluorosulfonic acid

PTFE = poly(tetrafluoroethylene)

QA = quaternary ammonium

PPO = poly(phenylene oxides)

IEC = ion-exchange capacity

BTMA = benzyltrimethyl ammonium

λ or ω = hydration number

SAXS = Small-Angle X-ray Scattering

FTIR = Fourier Transform Infrared

DMSO = dimethylsulfoxide

FWHM = full width half maximum

RM = reverse micelles

NP = nonylphenyl polyoxyethylene

AOT = anionic sodiumbis (2-ethylhexyl) sulfosuccinate

CTAB = cetyltrimethyl ammonium bromide

$TBAN_3$ = tetrabutylammonium azide

MeOH = methanol

NBS = *N*-bromosuccinimide

AIBN = azobisisobutyronitrile

NMP = *N*-methylpyrrolidone

RH = relative humidity

MCT = mercury-cadmium-telluride

LIST OF FIGURES

LIST OF TABLES

ACKNOWLEDGEMENTS

I would like to give thanks to my advisor, Dr. Michael A. Hickner, for his guidance, support and patience over these two years. Thank you for the opportunity of joining your group and being sent to conferences, which have helped shaped me into a better researcher and presenter of science. I also appreciate how you gave me the space to conduct my own research, while also steering me in the best direction.

I would also like to give thanks to the members of the Hickner group for being such good friends and helping me along the way. Thanks to Dr. Douglas Kushner and Dr. Tawanda Zimudzi for showing me the ropes in the lab and teaching me the tips and tricks of the trade. I could not have asked for better mentors. Many thanks to Dr. Liang Zhu for synthesizing the polymers I have utilized in this thesis work (Before you leave, can you prepare a new batch of polymers?). Thanks to Harrison Cassady, who made mundane lab work feel more enjoyable while listening to his stories of “great adventures”. Also, thanks to Clara Capparelli, and her husband Junior, for keeping the Spanish vibe alive and singing Spanish songs. I am also grateful to the rest of the group members for their friendship.

I would like to acknowledge my gratitude to all of the new friends I have made since being in Material Science. We passed some difficult classes all together. Thanks to all for adding a little more than just work in my life, even if it is just having dinner (more Chicken and Gnocchi soup, please!).

Finally, but not less importantly, I would like to give thanks to my family back home in Puerto Rico (enjoying the warm weather). They have been a great support for the

ups and downs during these two years. Thanks to my grandmother Virginia, for making such delicious food every time I visit (and basically ruining my palate since everything else is not as tasty). Thanks to my sister Larissa, for sending me *snapchat* pictures of our dog Uni. I miss that little *Bessie*! Thanks to my dad Frank, who have always encouraged me to do my best and “never give up”. Thanks to my mom Deana, for her unconditional help as my guidance counselor.

Chapter 1

Introduction

1.1 Background

In recent years, much effort has been invested in the development of environmentally friendly and renewable energy technologies. A potentially significant contributor for achieving the goal of clean, affordable and secure energy has been recognized in fuel cells, especially since they are highly efficient compared to combustion engines.[1] In fact, it is the mission of the Fuel Cell Technologies Office (FCTO) from the U.S. Department of Energy to support the research, and development of these technologies in order to facilitate their widespread commercialization.[2] One of FCTO's research priority is polymer electrolyte fuel cells (PEFC) technology,[2] which is considered an important component for viable power sources for mobile (automotive) and stationary use, water electrolyzers for hydrogen production, redox-flow batteries for large-scale energy storage, and reversed electrodialysis for energy production.[3]

All these electrochemical energy conversion systems depend on polymer ion-exchange membranes that separate and transport ions between the anodes and cathodes. The PEFC offers the advantage that this solid "electrolyte" is chemically bound within the polymer matrix and it consists of a thin polymer sheet, typically in the 25μm range. However, these PEFCs must fulfill specific requirements, such as: highly selective ion conductivity, chemical/thermal/dimensional stability, mechanical toughness, and long-

term durability. As a consequence, the properties of the ion-exchange membranes directly determine the performance, lifetime, and cost of the PEFC systems.

A polymer membrane that contains anionic side chains covalently bound to or embedded in a polymer backbone and selectively allows the passage of H^+ is termed a proton exchange membrane (PEM). If the polymer membrane contains positively charged side chains and selectively allows the passage of OH^-, it is called an anion exchange membrane (AEM). Of the two, PEMs are better known because they have a longer history and have received stronger commercial interest. Because of the highly acidic nature of the membrane, PEMs require the use of a precious metal catalyst (platinum) for stability and efficiency considerations, and thus, their expense often hinders widespread applications. This dependence on expensive electrocatalysts and the lack of fuel flexibility (other than hydrogen) are two significant drawbacks of the current PEM fuel cell technology, and these shortcomings have motivated an increasing interest in alkaline membrane fuel cells.

In contrast to PEMs, the alkaline environment in an AEM allows for the use of a range of low cost non-precious-metal catalysts and a wider choice of fuels. In addition, it is possible to even consider hydrogen fuels containing substantial amounts of impurities. Furthermore, the use of an AEM as a solid electrolyte prevents precipitation of carbonate/bicarbonate salts (a problem seen in alkaline fuel cells with a liquid electrolyte). For all of these reasons, AEMs have been attracting attention, and potentially inspiring the next generation of cheaper fuel cell technologies. Although AEMs have been used for decades now as separation membranes for several processes, such as: seawater desalination, metal ion recovery, electrodialysis and bioseparation,[4] they were

not considered stable or conductive enough to be applied in fuel cell technology, until 2005.[5] Unfortunately, AEM performance in terms of power output, stability and lifetime is still below PEM technology.[6] Major challenges in the development of AEMs remain on improving conductivity and enhancing alkaline stability.

Currently, the research community in AEM technology is intensely searching for improved, alkaline-stable, cationic polymers. One of the most promising approaches to emerge is the design and synthesis of cationic polymers with various side chain arrangements showing improved microphase separation, hydroxide ion conductivity and alkaline stability.[3] However, the challenge still remains to study the conformation and aggregation of these side chains and clarify the specific mechanisms behind their positive effects on conductivity and stability.

Prior work from the Hickner Research Group on a series of cationic poly(2,6-dimethylphenyleneoxide) (PPOs) functionalized by quaternary ammonium (QA) groups with different lengths of alkyl side chains[7,8] provided the material on which to perform this thesis work. These "comb-shaped" QA-PPOs were already reported to have improved anion conductivity and alkaline stability[7] based on the long alkyl chain that induced hydrophilic−hydrophobic separation (enhancing ionic conductivity), and reduced the nucleophilic attack of water or hydroxide (resulting in alkaline stability).[8] However, further issues on the relationships between molecular structure/morphology, membrane properties and water dynamics remain to be explored.

1.2 Motivation, Importance and Focus

A particular interest in better understanding the dynamics of water absorbed into AEMs, and how the water/hydrogen bonding interactions within the polymer membrane promotes ionic transport has motivated the scope of this thesis work. Since water behavior and hydrogen bonding of water can be readily examined with the linear Fourier transform infrared (FTIR) spectroscopy by observing the OD stretch of dilute HOD in H_2O,[9] FTIR methods were selected as the instrument for this thesis work. Mechanistic understanding of water dynamics/interactions in PEMs have been amply described in the scientific literature; however, similar understandings in AEMs remain unexplored.[10] These water interactions in AEMs are important for understanding the measures that must be taken to improve AEM technology, highlighting the importance of this thesis work and the scientific gap that is being addressed by this work.

The lack of complimentary AEM studies could be attributed, in part, to the inadequacy of OD as a probe for positively charged membrane systems. Consequently, another type of probe was required and the azide probe was selected, representing the "vehicle" for this thesis work. Since most of existing body of knowledge on the azide anion exists on its interactions with water, less on its use as a vibrational probe, and none as a probe to measure the hydration behavior in AEMs, this represents an innovative approach.

The focus of the work was to measure the hydration of cationic QA-PPO polymers with FTIR spectroscopy using the azide anion as a vibrational probe. It is hypothesized that the spectral features of the azide probe will render information on the

hydrogen bonding environment of water from the azide peak position and different water interactions with each QA-PPO.

1.3 Order of Information in the Thesis

The following chapters will cover a literature review of all related aspects that frame this thesis work in Chapter 2 and the *Materials and Methodology* in Chapter 3. The *Results and Discussion* is presented together in Chapter 4, where the necessary explanations will immediately follow the data being presented, to ensure better comprehension. Finally, the *Conclusions and Future Work* is discussed in Chapter 5. Additional data is presented in Appendix A on Contact Ion Pairs Observed in Sodium Azide, Appendix B on Parameters Determined from the Azide Band in the Four Sets of Mixtures, Appendix C on QA-PPO in N_3^- Form and Appendix D on Azide and Different Counter Ions.

1.4 References

(1) Kreuer, K.-D. Fuel Cells, Introduction. In *Fuel Cells: Selected Entries from the Encyclopedia of Sustainability Science and Technology*; Kreuer, K.-D., Ed.; Springer New York, 2013; pp 1–7.

(2) Miller, E. L.; Papageorgopoulos, D.; Stetson, N.; Randolph, K.; Peterson, D.; Cierpik-Gold, K.; Wilson, A.; Trejos, V.; Gomez, J. C.; Rustagi, N.; Satyapal, S. U.S. Department of Energy Hydrogen and Fuel Cells Program: Progress, Challenges and Future Directions. *MRS Adv.* **2016**, *1* (42), 2839–2855.

(3) Jannasch, P.; Weiber, E. A. Configuring Anion-Exchange Membranes for High Conductivity and Alkaline Stability by Using Cationic Polymers with Tailored Side Chains. *Macromol. Chem. Phys.* **2016**, *217* (10), 1108–1118.

(4) Slade, R. C. T.; Kizewski, J. P.; Poynton, S. D.; Zeng, R.; Varcoe, J. R. Alkaline Membrane Fuel Cells. In *Fuel Cells: Selected Entries from the Encyclopedia of Sustainability Science and Technology*; Kreuer, K.-D., Ed.; Springer New York, 2013; pp 9–29.

(5) Varcoe, J. R.; Slade, R. C. T. Prospects for Alkaline Anion-Exchange Membranes in Low Temperature Fuel Cells. *Fuel Cells* **2005**, *5* (2), 187–200.

(6) Merle, G.; Wessling, M.; Nijmeijer, K. Anion Exchange Membranes for Alkaline Fuel Cells: A Review. *J. Memb. Sci.* **2011**, *377* (1–2), 1–35.

(7) Li, N.; Yan, T.; Li, Z.; Thurn-Albrecht, T.; Binder, W. H. Comb-Shaped Polymers to Enhance Hydroxide Transport in Anion Exchange Membranes. *Energy Environ. Sci.* **2012**, 7888–7892.

(8) Li, N.; Leng, Y.; Hickner, M. A.; Wang, C. Highly Stable, Anion Conductive, Comb-Shaped Copolymers for Alkaline Fuel Cells. *J. Am. Chem. Soc.* **2013**, *135* (27), 10124−10133.

(9) Waldron, R. D. Infrared Spectra of HDO in Water and Ionic Solutions. **1957**, *809*.

(10) Marino, M. G.; Melchior, J. P.; Wohlfarth, A.; Kreuer, K. D. Hydroxide, Halide and Water Transport in a Model Anion Exchange Membrane. *J. Memb. Sci*. **2014**, *464*, 61–71.

Chapter 2

Literature Review

2.1 Introduction

This chapter covers a literature review of all related aspects that frame this thesis work, which particularly focuses on measuring the hydration of cationic polymers with Fourier transform infrared spectroscopy using the azide anion as a vibrational probe. However, to place this individual study into perspective, it is best to start with the "bigger picture", i.e., fuel cell technology. The importance and progress of fuel cells as a clean alternative energy conversion technology are addressed, as well as the materials-related challenges that still remain. Afterwards, general concepts of fuel cells are discussed to highlight how they are inherently more efficient than the current technology of internal combustion engines, followed by a short list of fuel cell families that have some technical relevance. This literature review then offers more information on polymer electrolyte fuel cells by comparing and contrasting proton exchange membranes and anion exchange membranes. Finally, the literature review then narrows down and goes into more depth on anion exchange membranes, culminating with an explanation of the "comb-shaped" cationic polymers specifically utilized for this thesis work.

Knowing the importance of understanding the dynamics of water absorbed into polymer membranes for energy applications, which is the scope of this thesis work, a discussion of the literature regarding basic studies of water hydrogen bonding in proton

exchange membranes is presented. Most of this background discussion relies on work that was conducted on proton exchange membranes. Similar understandings of water dynamics in the anion exchange membrane counterparts remain unexplored in the literature, representing a scientific gap that is being addressed in this thesis work.

Having selected the azide anion probe as the vehicle to measure hydration behavior, a focused discussion of the literature regarding the azide anion is then presented. Most of the existing body of literature addresses the azide's interactions with water, less on its use as a probe, and none on its use as a probe in anion exchange membrane experimental systems. Thus, this work takes an innovative approach to elucidating the behavior of anion exchange membranes using a vibrational probe.

2.2 Perspective on Fuel Cells

Environmental, geo-political, and economical concerns have been promoting the development of novel technologies that can provide clean alternative fuels derived from renewable sources and safe, large-scale energy storage. Fuel cell technologies have seen a revival in recent years because they have been recognized as having the potential of being a significant contributor in meeting the national goals to reduce greenhouse gas emissions and petroleum use and to enable the availability of clean, affordable and secure energy. A unique feature of fuel cells is that in spite of being compact, they have high fuel efficiency, which contrasts with heat engines that only reach high efficiencies in very large units (Fig 2.1). Moreover, fuel cells use energy dense chemical fuels that have a large advantage over batteries that have relatively lower energy density. Areas of major

interest for efficient conversion technologies are for mobility, combined heat and power systems, and portable electric and electronic applications.[1]

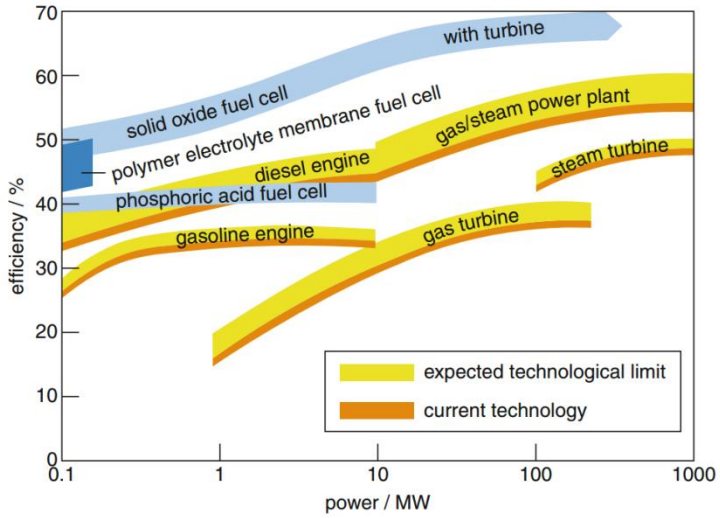

Fig. 2.1 Efficiency vs. power for different fuel cell types compared to other energy technologies.[1]

Only recently have fuel cell technologies begun to shift from the fundamental research to real-world applications. After decades of research and generations of prototypes, 2015 saw the first commercial fuel cell electric vehicle in history being sold to regular customers.[2] In fact, it is the mission of the U.S. Department of Energy's Fuel Cell Technologies Office (FCTO) to support the research, development, and demonstration of hydrogen and fuel technologies to facilitate their widespread commercialization. FCTO efforts are intended to accelerate progress toward specific techno-economic targets in fuel cells by 2020, which should enable reductions of 2-4 million barrels of oil used per day and 200-450 million metric tons of greenhouse gases per year in the U.S. So far, FTCO activities have resulted in a 50% decrease in fuel cell cost since 2006, and an 80% cost reduction for electrolyzers since 2002. Despite this progress, many challenges remain in fuel cell technology, most of which are materials

related. The FCTO's research priorities are focused on polymer electrolyte fuel cells (PEFC), but also include alkaline fuel cell (AFC) technology as future-generation technology.[2]

The idea of directly generating electricity from chemical fuels using fuel cells is not recent. During the early 19th century, the concept of fuel cell was demonstrated by Humphry Davy (1801), then followed the basic investigation of Christian Friedrich Schönbein (1838) on the reactions of H_2 gas and O_2 gas dissolved in the electrolyte at an electrode/electrolyte interface, which is the fundamental fuel cell reaction.[3] Later, William Robert Grove (1842) designed and constructed the first operating fuel cell, using H_2 as fuel, O_2 as oxidant, platinum as the catalyst and sulfuric acid as the electrolyte.[4] Nowadays, several different types of fuel cell families have been developed; however, they all have in common the basics: two electrodes (the anode and the cathode) and the electrolyte that separates them.

2.3 General Concepts in Fuel Cells

A fuel cell is an electrochemical device that converts the chemical energy stored in gaseous or liquid fuel directly into work of electrical energy at a constant temperature (Fig. 2.2). This direct energy conversion calls attention to one of the advantages of fuel cells; i.e., by converting chemical potential energy directly into electrical energy, fuel cells are inherently more efficient than combustion engines, which must first convert chemical potential energy into heat, and then mechanical work.[4]

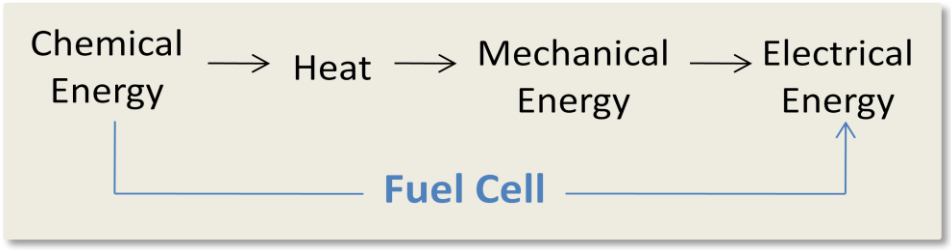

Fig. 2.2 Schematic representation of direct energy conversion in an electrochemical cell as compared to thermal conversion in an internal combustion engine.[4]

In a fuel cell, the fuel (e.g., hydrogen, methane, methanol, or ethanol) is oxidized at the anode, generating electrons that are donated at the cathode to an oxidant (e.g., oxygen), which is reduced. Each of the two electrode reactions creates a characteristic potential difference, traveling from anode to cathode, across the interface solid electrode/electrolyte. The chemical energy released at each, locally separated, electrode is directly transformed into electrical energy, which is directed through electronic connectors at both electrodes to an external circuit that contains the operable electrical device. Both electrochemical interfaces are in a common electrochemical cell and joined by a common medium, an ion-conducting electrolyte.

Since fuel cells are open systems, fuel and oxidant gas are supplied from their respective tanks (i.e., if oxidant is pure oxygen) through the fuel cell housing to the electrodes. The gases pass through the porous gas diffusion layers (GDLs), typically of μm range, towards the electroactive catalystic layers (ECL) at the interface of the electrolyte (Fig. 2.3). The GDL and ECL together are often referred to as the gas diffusion electrode (GDE).

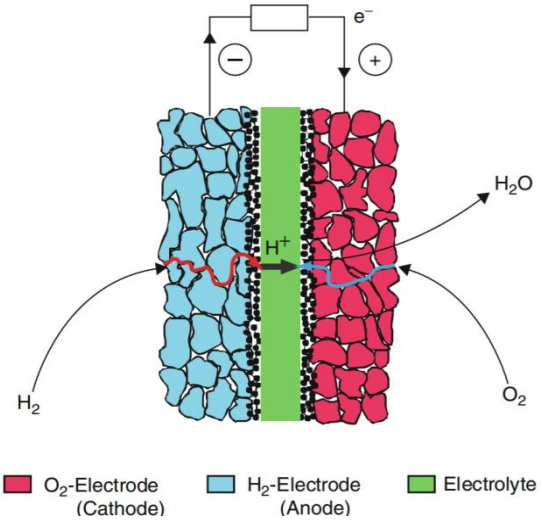

Fig. 2.3 Simplified polymer electrolyte fuel cell (PEFC), showing only the porous gas diffusion electrodes and electrolyte, cell housing is not shown. Fuel: H_2, oxidant: O_2.[4]

An example of the electrochemistry of the electrode reactions is the combustion of H_2 with O_2 to H_2O, where two partial reactions occur at the two different electrodes:

Anodic reaction: $\mathbf{H_2 = 2H^+ + 2e^-}$ (hydrogen oxidation reaction, HOR) (2-1)

Cathodic reaction: $\mathbf{½O_2 + 2H^+ + 2e^- = H_2O}$ (oxygen reduction reaction, ORR) (2-2)

Overall reaction: $\mathbf{H_2 + ½O_2 = H_2O}$ (2-3)

Having only water and heat as the reaction products calls attention to another advantage of fuel cells, and it represents a huge improvement over the multiple emissions of greenhouse gases from internal combustion engines.

The voltage of each cell is generally only 0.8-1.1 V. To accumulate the voltage for technical applications (e.g., 200-400 V) fuel cells must be connected in series, called a fuel cell stack, which combines individual cells to an electrical series connection with distributed mass flowing through the device. With the mass flow of reactants into and

products out of the fuel cell stack, a cooling system is needed to remove the waste heat. In systems where oxygen is derived from air (air-fed fuel cell), the ambient air must be processed (cleaned, humidified, etc.), which gives an advantage of eliminating weight and volume from the device.

The design of a fuel cell system must tackle issues of mass and heat transfer, current distribution across the cell, voltage distribution along the stack, and the type of application (e.g., mobile, stationary or portable). Ultimately, the design is guided by the fuel cell type (Fig.2.4).

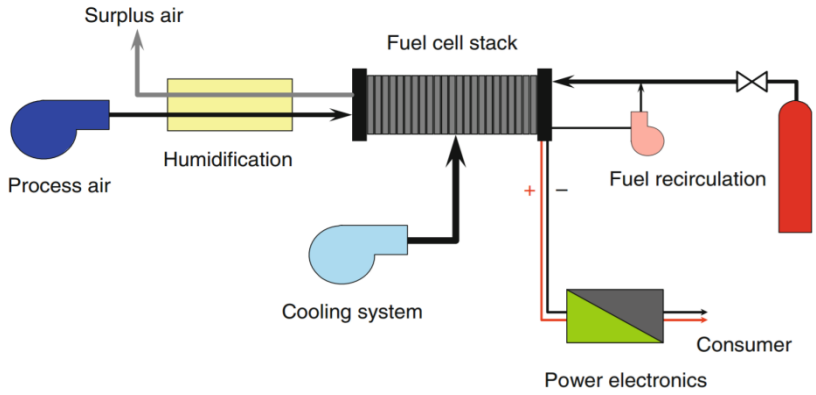

Fig. 2.4 Simplified fuel cell system.[4]

2.4 Fuel Cell Families

The fuel cell types having some technical relevance are presented schematically in Fig. 2.5. However, this review will not discuss all of them; only the most pertinent. Fuel cells are usually classified: by their temperature of operation and/or, more frequently, by the nature of the electrolyte (acidic or alkaline).

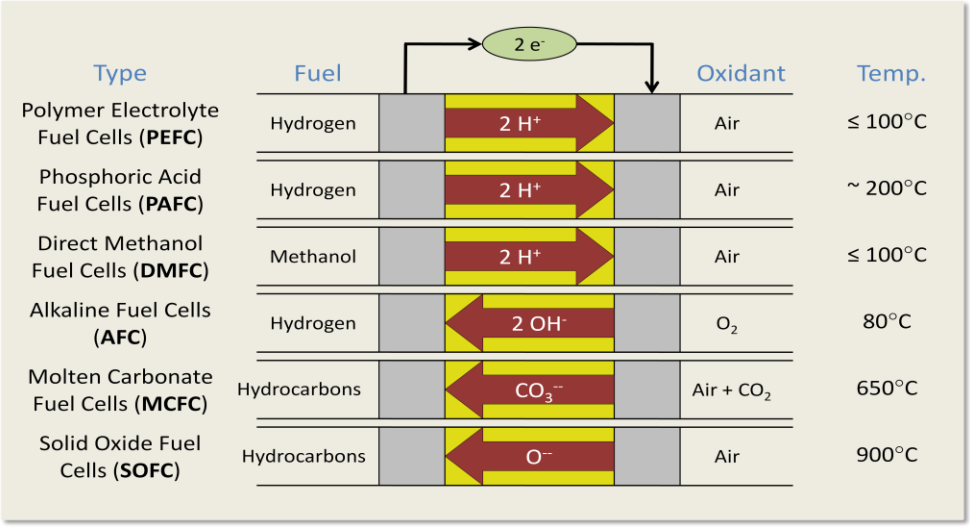

Fig. 2.5 Important fuel cell families of today.[4]

In acidic electrolytes, the ionic conduction is provided by H^+ ions, created by the anodic oxidation of H_2 fuel, and transported to the cathodic reduction of O_2, and water as the reaction product appears at the cathode side of the cell, as in the previously presented electrochemical reactions (Eq. 2-1 to 2-3). For fuel cells with an acidic electrolyte, platinum is the electrocatalyst of choice at temperatures up to 200 ^oC (e.g., phosphoric acid fuel cell, PAFC).

In alkaline solution, the ionic conduction is provided by OH^- ions, created by the ORR at the cathode. OH^- ions are carriers for the O_2^- ions, produced by the cathodic reduction reaction of O_2 and the follow-up reaction with a water molecule. After conduction, OH^- reacts with the H^+ created at the anode and yields water as a product at the anode side. The electrochemistry of HOR and ORR is written as follows:

Anodic reaction: $\mathbf{H_2 + 2OH^- = 2H_2O + 2e^-}$ (hydrogen oxidation reaction, HOR) (2.4)

Cathodic reaction: $\mathbf{½O_2 + 2H_2O + 2e^- = 2OH^-}$ (oxygen reduction reaction, ORR) (2.5)

Overall reaction: $\mathbf{H_2 + ½O_2 = H_2O}$ (2.6)

Initial concepts for an alkaline fuel cell (AFC) were described with an aqueous alkaline electrolyte (NaOH or KOH solution), where they became of interest because alkaline electrolytes allowed cheaper, non-precious metal catalysts, such as nickel, its alloys and silver.[5,6] Alkaline fuel cells with an aqueous electrolyte require pure H_2 and O_2, because CO_2 from the air or the oxidation product of the fuel led to progressive carbonation, formation of $NaCO_3$ or K_2CO_3 precipitates, and eventually reduction of its performance.[7] This CO_2 problem hindered its further development, but it is being addressed with the more recent progress in the preparation of alkaline anion exchange membranes (AEM).[8]

Taking into account the double function of the electrolyte (i.e. transporter of ionic charge and separator), the concept of having a solid electrolyte fulfill both functions at the same time led to the use of a solid polymer electrolyte. Using thin ion-conducting polymer membranes as electrolytes gave way to a different concept of a fuel cell, usually called polymer electrolyte fuel cell (PEFC).

2.5 Polymer Electrolyte Fuel Cells

In comparison to fuel cells with a liquid electrolyte, the PEFC concept offers the advantage that this “electrolyte” is chemically bound within the polymer matrix and only

water as reactant, in addition to the gases, appears in the peripheral system components. This solid "electrolyte" consists of a thin polymer sheet, typically in the 25μm range. A polymer membrane that contains anionic side chains covalently bound to or embedded in a polymer backbone, selectively allowing the passage of H^+, is termed a proton exchange membrane (PEM). If the polymer membrane contains positively charged side chains, selectively allowing the passage of OH^-, it is called an alkaline anion exchange membrane (AAEM) or anion exchange membrane (AEM) for short (Fig. 2.6).

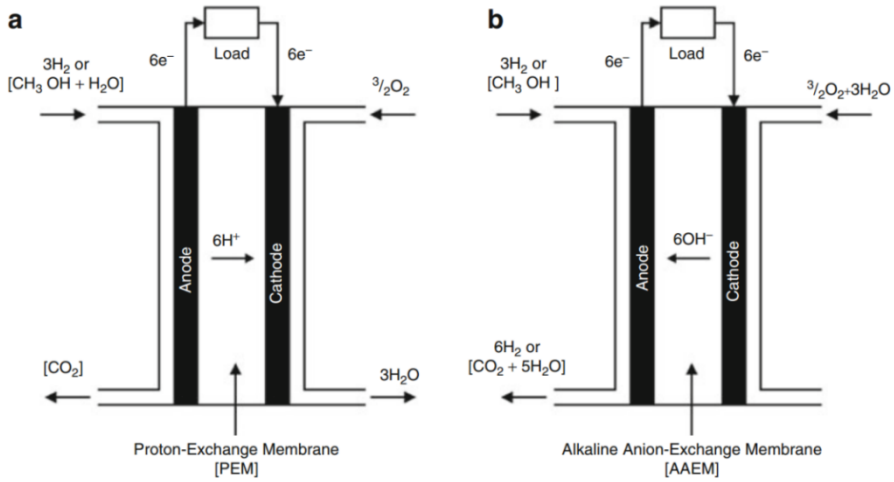

Fig. 2.6 Schematic presentation of PEM(a) and AEM(b) both fueled with H_2 gas or methanol. The stoichiometric ratios of reactants and products are shown.[9]

Of the two, PEMs are better known because they have a longer history, and have received stronger commercial interest. H_2-fed PEM fuel cells were first used by NASA's Gemini Program in the 1960s to provide auxiliary power for the space vehicles and drinking water for the astronauts.[10] Still today, pure hydrogen is considered the ideal fuel and H_2-fed PEM fuel cells are the most commercially developed for electric vehicles,

which are expected to compete commercially with internal combustion engines by 2020.[2] Because of the highly acidic nature of the membrane, PEMs require the use of a precious metal catalyst (platinum) for stability and efficiency considerations, and thus, their expense often hinders widespread applications. Platinum nanoparticles, typically a few (3-5) nanometers in diameter, are supported on various carbon substrates (e.g., 20-40% Pt/C), with typical Pt loadings of ca. 0.1 mg/cm^2 at the anode side and ca. 0.4 mg/cm^2 at the cathode side, to serve as the electrocatalyst.[4] To reduce material costs, one of the research and development efforts are on reducing platinum group metal (PGM) loading, intending to achieve ultra-low-PGM and PGM-free catalysts with increased activity and durability.[2] For H_2-fed PEMs, membranes are perfluorinated or partially fluorinated polymers, with side chains ending in pendant acid groups (e.g. the sulfonic acid group – SO_3H). The first reported ion-conducted membrane in the 1960's by DuPont was Nafion®, a perfluorosulfonic acid (PFSA) ionomer.[11] Nafion® has a hydrophobic poly(tetrafluoroethylene) (PTFE) backbone with randomly distributed ether-linked pendant side chains containing hydrophilic sulfonic acid head groups. Since then, PFSA has received much attention in research, found widespread applications, and inspired the development of a series of chemically similar polymers with different side chain lengths while retaining the same PTFE backbone. However, these PFSA-based PEMs all require water to facilitate the dissociation and transport of protons. Under operation, the PEM has to contain some water (e.g., 15 water molecules per sulfonic acid group) to provide the necessary specific conductivity. This fact causes consequences for the fuel cell system design; since hydrogen gas and air have to be humidified before flowing into the cell to sustain the hydration level in the membrane. Overcoming this need for fully humidified

reactants, and simplifying the fuel cell system design, represents another research focus: attaining PEMs capable of proton conductivity at low relative humidity and functioning under drier operating conditions.[2,12]

In contrast to PEMs, the alkaline environment in an AEM allows for the use of a range of low cost non-precious-metal catalysts. In addition, it is possible to consider hydrogen fuels containing substantial amounts of impurities. Furthermore, the use of an AEM as a solid electrolyte prevents precipitation of carbonate/bicarbonate salts (a problem seen in alkaline fuel cells with liquid electrolyte). For all of these reasons, AEMs have been attracting attention, and potentially inspiring the next generation of cheaper fuel cell technologies. However, performance in terms of power output and stability/lifetime is below PEM acidic technology.[8] AEMs will be discussed further in the next section.

A common problem to all polymers for the different fuel cell types is to generate an optimal electrolyte/electrode interface. The gas reactants are converted into ionic species, solvated/hydrated in the electrolyte, by exchanging electrons with the electrode. This reaction occurs at the three-phase boundary, where electron conducting, ion conducting, and gas phase join to each other. To allow a high surface area for the generation of a current, the electrolyte/electrode interface is extended into a three-dimensional interphase with a certain thickness. A schematic of this interphase at the PEFC cathode (oxygen) side is shown at Fig. 2.7. This 3D interphase has to be established during the preparation and manufacturing procedure of each solid electrolyte material for the different fuel cell types.

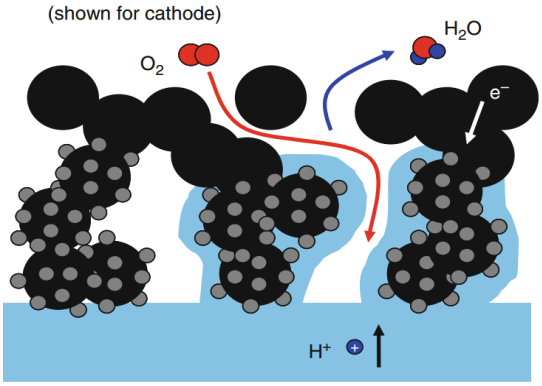

Fig. 2.7 Electrode layer interphase with three phase boundary of a PEFC (cathode side). *Blue*: polymer electrolyte, *black*: carbon particles, *gray*: platinum nanoparticles.[4]

2.6 Anion Exchange Membranes

AEMs are polymer electrolytes that conduct anions, such as OH^- and Cl^-, because they contain positively charged (cationic) groups tethered to the polymer backbone. AEMs have long been used, for five decades now, as separation membranes for several processes (e.g., seawater desalination, metal ion recovery, electrodialysis and bioseparation).[9] However, they were not considered stable or conductive enough to be applied in fuel cell technology, until favorably discussed in a review by Varcoe, et al. in 2005.[13] At that time, Yu and Scott had just reported the use of a commercial AEM, i.e. Morgane®-ADP membrane (Solvay, S.A.), made from cross-linked per-fluorinated backbones and quaternary ammonium (QA) moieties as ion exchange groups, for their application in direct methanol fuel cell technology.[14] Earlier AEMs developed by the Tokuyama Soda Company in Japan, used poly(chloropropene) crosslinked with divinylbenzene, which were subsequently functionalized with quaternary ammonium groups using triethylamine.[14]

The standard synthesis of AEMs typically involves chloromethylation of aromatic rings or bromination on benzyl methyl groups of a polymer, then reaction with a tertiary amine, which then results in polymers with QA groups randomly distributed in benzylic positions along the backbone (illustration shown at Fig 2.8 **a**). However, in this configuration, having the QA groups directly on the stiff aromatic polymer backbone restricts their local mobility and impedes the efficient phase separation of ionic cluster domains, which are necessary for formation of hydrophilic channels for the transport of water and anions. How the different configurations of the polymer side chains affect the conductivity and stability of the AEMs was discussed by Jannasch and Weiber.[15]

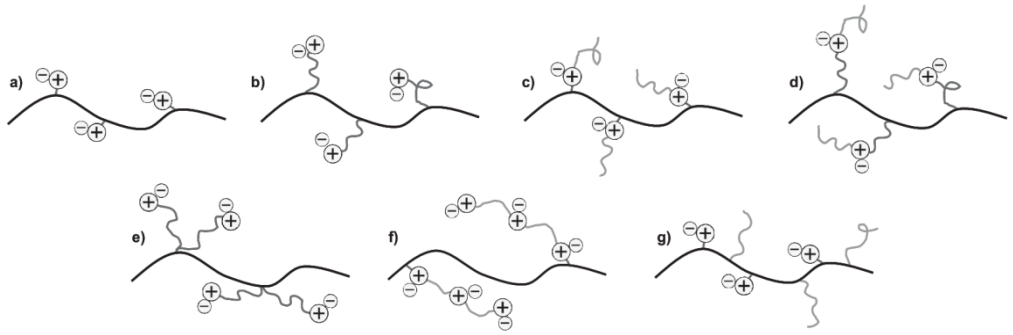

Fig. 2.8 Different strategies to attach the cationic groups to the polymer backbone with side chains: a) directly on the backbone, b) via spacer chains, c) directly on the backbone with extender chains pendant to the cations, d) via spacer and extender chains, e) via spacer chains in pairs, f) multiple cations via connecting chains, and g) directly on the backbone with separate side chains.[15]

For widespread AFC applications, AEMs ideally require certain important properties, which include high ion conductivity, chemical, thermal and dimensional stability, mechanical toughness and long-term durability.[15] In this regard, AEMs currently lack the combination of high OH^- conductivity with sufficient stability under alkaline conditions.[8,16] Being highly basic and nucleophilic, OH^- is responsible for the

attack and degradation (hydrolysis) of ion-exchange groups, such as QA, as well as the polymer backbones. Several types of degradation seen in different QA groups include: β-hydrogen Hofmann elimination, direct nucleophilic substitution at an α-carbon, and elimination by way of ylide formation.[15,16] Furthermore, during operating conditions of the AEM, OH^- is neutralized by the rapid absorption of CO_2 (upon exposure to air), which causes the detrimental formation of bicarbonate/carbonate. Therefore, a system with high, long-term alkaline stability of above 80°C is preferred, because at these temperatures bicarbonate/carbonate formation is impeded.[15]

Several QA groups in benzylic positions have been proven to be sensitive towards nucleophilic attack, and seeking to improve the alkaline stability, a number of different cationic groups (e.g. imidazolium, pyridinium, guanidinium and phosphonium) have been attached to different polymer backbones and investigated as AEMs with varying results.[17] Another focus of investigation has been the polymer backbone itself, of which the most commonly studied have been poly(sulfone),[16] poly(ether ketone),[18] poly(ether imides),[19] poly(phenylene oxides)[20] and those based on poly(styrene).[21] For some time now, Tomoi, et al.[22] reported an enhanced alkaline stability by inserting a flexible alkyl chain in between the poly(styrene) backbone and the QA groups (illustration shown at Fig 2.8 **b**). More recently, Hibbs studied poly(phenylenes) with attached QA groups through hexyl spacers, demonstrating excellent stability in 4M KOH at 90°C, with only a 5% loss of conductivity over 336 h and no loss of ionic content.[23] These results have led way to the research and development of several cationic polymer structures with different kinds of side chain configurations, and using different backbone polymers and synthetic pathways for AEM purposes, as illustrated in Fig 2.8.

This thesis work specifically utilized "comb-shaped" polymers, based on the works of Li[20] and Hickner[24], from a series of poly(phenylene oxides) (PPOs) functionalized by QA groups with different lengths of alkyl side chains (illustration shown at Fig 2.8 **c**). These quaternary ammonium PPOs (QA-PPOs) were designed to modify the sterics around the nitrogen center and the hydrophobicity of the ammonium cation. An important finding was that by introducing one long alkyl chain of up to 16 carbon atoms pendant to the cationic center formed a comb-shaped structure; and this comb-shaped structure induced microphase separation (enhancing ionic conductivity), mitigated water swelling of the membrane, and reduced the nucleophilic attack of either water or hydroxide at the QA (resulting in good alkaline stability).[20] To improve upon their mechanical properties, the research group tuned the number and length of alkyl side chains with the purpose of developing a new polymer system that would support high ion-exchange capacity (IEC) values (i.e., high hydroxide conductivity), while maintaining good material properties and alkaline stability. The series of comb-shaped QA-PPOs were termed **CyDx**, where **y** refers to the length of alkyl chain and **x** refers to the number of degree of bromination, e.g. **x** = 40 representing an average of 0.4 bromomethyl groups per PPO repeat unit (Fig 2.9).

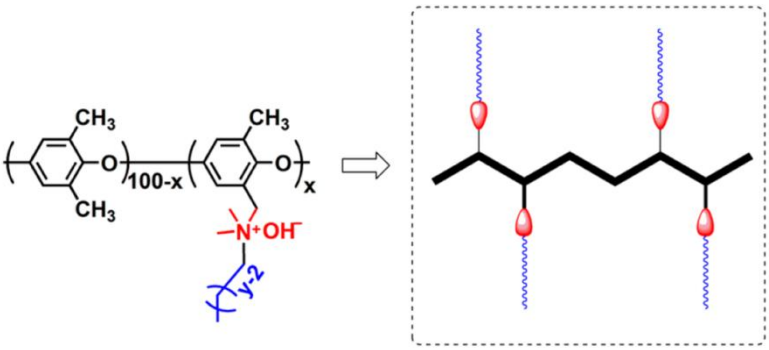

Fig. 2.9 Comb-shaped CyDx polymer, where x=40.[24]

Continued work by Hickner's group measured ionic conductivities, microphase-separated structures, and alkaline stabilities on the series of QA-PPOs and compared them to the PPO with benzyltrimethyl ammonium (BTMA) cations[20,24] (illustration of BTMA shown at Fig 2.8 **a**). These polymer membranes were found to exhibit excellent solubility in pure methanol, ethanol and *n*-propanol, but were insoluble in pure water (even at 80°C), demonstrating their usefulness as catalyst layers without suffering losses by solubility.[24] Characterization of these polymers by ^{1}H NMR spectroscopy obtained the IEC values from the spectrum, which were shown to be similar to the titrated gravimetric IEC values.[24] Kushner, et al.[25] studied the water uptake and consequent mechanical influences in confined comb-shaped polymers in both bulk membrane and thin film forms. The hydration number (λ), defined as:

$$\lambda = \left(\frac{\Delta m}{m_{dry}}\right)\left(\frac{1000}{M_{water} * IEC}\right) = \frac{[H_2O]}{[QA^+]} \tag{2.7}$$

where m_{dry} is the dry mass, and M_{water} is the molar mass of water (18 g mol^{-1}); was used to correct the IEC differences of each polymer. In the bulk membrane (Fig 2.10 a), it was demonstrated that as the side chain length increased, the λ decreased; which was attributed to the reduction in IEC.[24–26] Morphology profiles of the polymers, as determined by small-angle X-ray scattering (SAXS), revealed characteristic ionic peaks, which indicate the presence of ionic clusters due to nanophase separation, that were moderate for BTMA40, C6D40 and C10D40, but very clear for C16D40. Upon testing for water uptake at room temperature, BTMA40 absorbed more water, having a higher IEC. The comb-shaped polymers displayed a lower water uptake relative to the increased length of the alkyl chain; longer alkyl chains showed stronger hydrophobicity, which

restricted the water absorption of the comb-shaped copolymers. When measuring the hydroxide conductivity, the comb-shaped polymers showed higher conductivity compared to BTMA40 under the same conditions. Thus, the comb-shaped polymers showed high hydroxide conductivity but lower hydration values (λ). The polymer with the longest alkyl chain (C16D40) showed slightly higher conductivity than the other samples. Accordingly, it is hypothesized that highly phase-separated, uniform ionic domains should transport hydroxides ions more efficiently, yielding high hydroxide conductivity.[20,24] Investigating the comb-shaped polymers for stability, demonstrated a slow decline in conductivity during the initial period of fast degradation, i.e. the first 200 h. After 2000 h of immersion in 1 M NaOH at 80°C, the comb-shaped polymers were able to retain ~80% of their conductivity, while the BTMA40 decreased to 40%. Overall, these initial findings of high conductivity, excellent alkaline stability, and low water uptake (with inconsequent dimensional swelling) have suggested that this comb-shaped architecture is a promising approach for the design of AEMs that meets the demanding challenge for alkaline fuel cells applications.

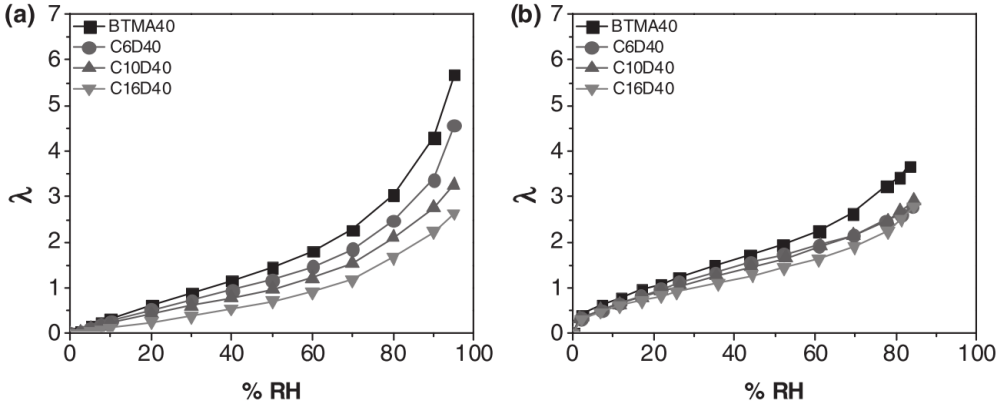

Fig. 2.10 Hydration number as a function of % relative humidity (RH) for: a) bulk membrane and b) thin films.[25]

2.7 Studies of Water Hydrogen Bonding in PEMs

Water is known for its amphotericity[27], its fast rotational dynamics[28] and its ability to form dynamic hydrogen bonds.[29] Accordingly, water plays a crucial role as a solvent in many different systems found in biology and chemistry. These systems do not often contain bulk water, but rather a limited number of water molecules within a confined environment. When water is confined, it can have a strong effect on the strength, structure, and mobility of the network.[30] More specifically, within polymer membranes for energy applications, it is important to understand the dynamics of water absorbed into the membrane. It has been hypothesized that regarding the function of hydrated PEMs and AEMs, the key aspect lies in the polymer interaction with water and how water characteristics in these membranes promote ionic transport.[31–34]

Water behavior and the hydrogen bonding of water can be readily examined by using the linear Fourier transform infrared (FTIR) spectroscopy and observing the OD stretch of dilute HOD in H_2O, a technique first employed by Waldron[35] with HOD to study the differences in hydrogen bonding lengths of various halide salts. The OD stretch refers to the stretching frequency of the covalent bond between oxygen and deuterium, where the frequency is indicative of the strength of the hydrogen bond. Diluted HOD in H_2O is used because it simplifies the spectrum of pure H_2O or D_2O by eliminating Fermi resonance and overlapping bands[36,37]. This allows for a single vibrational stretching mode to be analyzed.

Earlier studies by Fayer, et al.[31] evaluated the water dynamics in the PEM's Nafion® membranes. When Nafion® was hydrated with dilute HOD in H_2O, the

vibrational spectrum displays a broad, non-Gaussian peak at a range of ~2700-2400 cm^{-1}. This broad peak encompassed the distribution of hydrogen bonding environments that absorbed water experiences within the polymer, and the distribution could be rigorously deconvoluted to disclose the percentage of water in various microenvironments. They also studied varying levels of Nafion® hydration, in order to understand how the hydrogen bonding network varied as a function of water content. The researchers were able to develop a peak fitting routine comprised of the weighted sum of two water distributions and extract quantitative population values corresponding to the bulk water and polymer. Extensive studies on Nafion®[31] as well as related studies on water dynamics in reverse micelles[38,39] opened new areas of research opportunities.

More recent work on water dynamics was performed by the Hickner research group. Black, et al.[40] examined how backbone polarity and side-chain electron-withdrawing properties influenced water binding within two types of polymer membranes and a variety of sulfonate groups. The OD stretch peak was used on sulfonated syndiotactic poly(styrene) and poly(sulfone) films to extract the water population. In addition, the strength of the hydrogen bond formed between the sulfonated group and water based on the peak frequency of the OD stretch. Afterwards, Smedley et al.[41] used a three-population model derived from the previously used two-population core-shell model. The two-population model was developed for reverse micelle environments where there are only two types of water; water molecules that interact with the sulfonate headgroup (shell water) and bulk-like water that interacts with other water molecules (corewater).[38] This concept was then applied to water absorbed into Nafion® membranes due to its ability to strongly phase segregate, resembling somewhat a reverse micelle.

However, poly(styrene) based polymers do not phase segregate as strongly as Nafion® and the two-population model was altered to deconvolute the OD peaks. A third peak was added to the water population model to account for water in an intermediate population. There is significant evidence for this type of water in the literature (usually referred to as "loosely bound" water), where this water is not directly interacting with the sulfonate group, but are still affected having slower dynamics. Water in both the first and second hydration shells of the sulfonate group was accounted for by employing the three-population model. A schematic of the three types of water is shown below in Fig. 2.10.

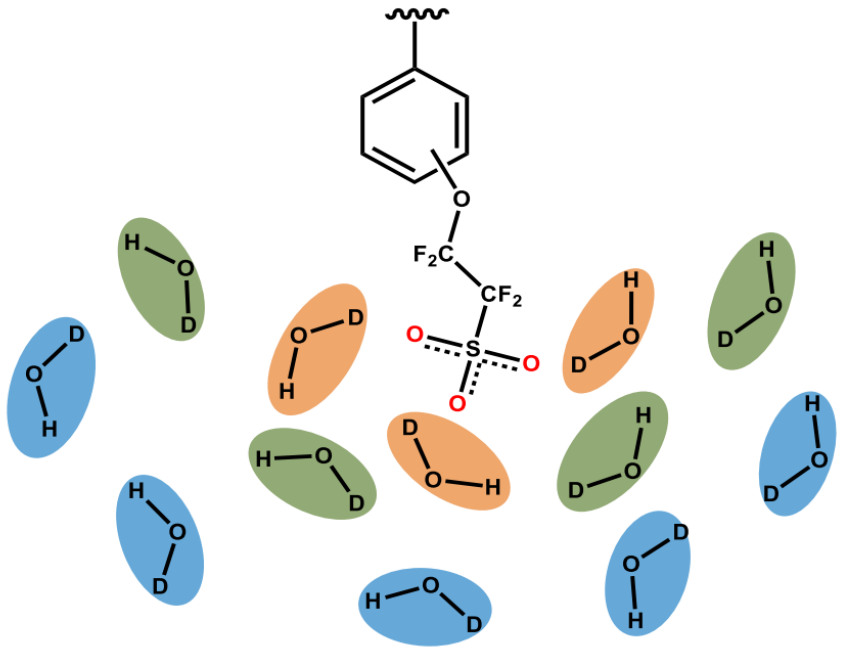

Fig. 2.11 Schematic of the different populations of water absorbed into the polymer membrane. Blue represent bulk water, green intermediate water and orange the water bounded to the sulfonate group.[41]

At present time, similar mechanistic understandings of water dynamics or interactions in AEMs remain unexplored in the scientific literature.[33] These water interactions in AEMs are important for understanding the measures that must be taken to

improve AEM technology. It is precisely this scientific gap that is being addressed by this thesis work. The lack of complimentary AEM studies could be attributed, in part, to the inadequacy of OD as a probe for positively charged membrane systems. Consequently, this work required another type of probe. The discussion that follows relates to the selection of the azide anion probe for this purpose.

2.8 The Use of the Azide Anion as a Vibrational Probe

A known methodology to investigate the equilibrium of free ions in non-aqueous solutions is the infrared spectroscopy (IR), where the internal vibrations of a polyatomic anion are often used as probes.[42] For example, pseudo-halide anions exhibit a strong IR band in the 2000-2200 cm^{-1} region, which is convenient for the characterization of ion pairs. Triatomic pseudo-halides can be separated in two groups according to their mechanical coupling: the first is exemplified by thiocyanate (SCN^-), and the second is exemplified by cyanate (OCN^-) and azide (N_3^-). For SCN^-, the mechanical coupling between CS and CN is moderate; the high frequency vibration υ_3 is close to a pure υ(CN) vibration at 2137 cm^{-1} while the low frequency vibration υ_1 is close to υ(CS) at 1030 - 1275 cm^{-1}. In the second group, this separation becomes inadequate in OCN^- and meaningless in N_3^-, which makes υ_3 almost twice as sensitive to inter-molecular interactions as compared to SCN^-. Consequently, OCN^- and N_3^- have been preferred to measure weak interactions caused by hydrogen bonding of proton donors.[42]

The azide ion (N_3^-) exhibits a very strong infrared ν_3 band in the 2000−2100 cm^{-1} region and can be used to characterize ion pairs and intermolecular interactions, including

hydrogen-bonding and ion-dipole interactions.[43] Furthermore, the azide ion is relative small (1.2 Å N-N bond length)[44] and its sodium salt is soluble in water. Because of these properties, numerous experimental studies have been performed with the azide ion in various media, such as in bulk homogenous solvents,[42,43,45–47] in reverse micelles,[48,49] and in biologically relevant systems.[50]

Le Borgne, et al.[42] studied azide ion pairs with alkali and alkaline earth metals cations in dimethylsulfoxide (DMSO) solvent by using FTIR spectroscopy and *ab initio* calculations. They found that the ν_3 vibration mode of N_3^- at 2000 cm^{-1} was sensitive to the nature of the metal ions and the frequency shifts for a given ion pair was related to the polarizing power of the metal ion. More recently, Son and collaboratres[43] did similar works, as shown in Fig. 2.12, which displays FTIR spectra of the asymmetric stretching band (ν_3) of free N_3^- ion and N_3^- in contact ion pairs in DMSO. The peak at ~2000 cm^{-1} results from free azide ion and its bandwidth (fwhm) is ~11 cm^{-1}. The peak position and width of the azide ion are dependent on its local environment. When azide ion (N_3^-) forms contact ion pairs with alkali metal and alkaline earth metal ions, the ν_3 mode of N_3^- is significantly blue-shifted and its bandwidth is increased, and the frequency shift of N_3^- in contact ion pairs is dependent on the cation used. When N_3^- is paired with Na in NaN_3, a shoulder appears in the azide ν_3 at 2024 cm^{-1} and when paired with Mg^{2+} in MgN_3^+ the azide ν_3 appears at 2057 cm^{-1}.

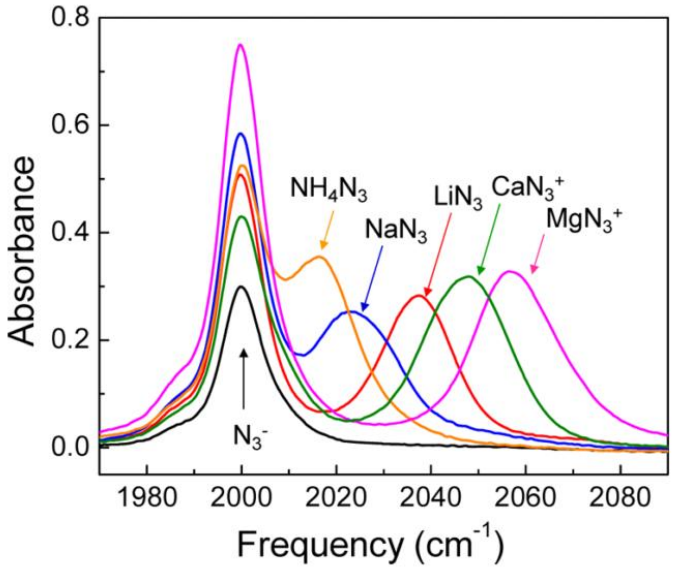

Fig. 2.12 FTIR spectra of the ν_3 band of N_3^- in DMSO. The peak at 2000 cm^{-1} is from free N_3^- ion, while at higher frequency peaks are from ion pairs.[43]

It has been discussed by researchers that the frequency shift of a vibrational probe in solution results from the vibrational solvatochromic effect.[43,51,52] Since the vibrational frequency of a solute in solution will vary according to the local electrostatic environment produced by the solvent molecules, the frequency shift of a vibrational probe depends on the detailed solvation structure. Lee, et al.[51] studied the vibrational solvatochromic effects of CN^-, SCN^-, and N_3^- in water, and found that the vibrational frequencies are dependent on the hydrogen bond length and angle between water and the ions. When contact ion pairs are in DMSO, the azide ion experiences a different local electrostatic field produced by both the cations and DMSO molecules. Sando, et al[45] characterized ionic liquids and water mixtures using FTIR and time-resolved IR pump-probe studies of the asymmetric stretching band of the azide anion as a probe for the solvent environment. They used azide in DMSO because it closely resembled the vibrational spectra and dynamics in ionic liquids. The researchers found that at low molar

fractions of water, two bands appeared in the spectra; in pure DMSO, a single band at 2000 cm^{-1} did not shift upon adding water, but disappeared over time. A band interpreted as the azide interacting with water, and designated as "wet" band, appeared at higher frequencies upon adding water (beginning at 2008 cm^{-1} at 0.02 molar fraction of water), and gradually blueshifted and gained intensity (2047 cm^{-1} at pure water). The researchers concluded that with the addition of water, a higher fraction of the anions have water penetrating into the first solvent shell. The probe frequency dependence observed for vibrational dynamics in the DMSO also indicated the mixed environment. In general, the frequency shift of azide ion in contact ion pairs is strongly influenced by the electrostatic interaction and relative geometry between the cations and azide ions.[52]

Research on reverse micelles (RM) have shown the value of the azide anion as a vibrational probe to investigate water interactions in confined structures by its widespread use in both static and ultrafast FTIR.[39,48,53–55] Studies on RMs, however, have shown that the azide ion is equally sensitive to changes in the hydrogen bonding environment for neutral, cationic and anionic systems.[48] Zhong, et al.[48] used the FTIR spectroscopy to observe the water OH stretching band, the headgroup CO stretching band and the ν_3 azide ion band using three types of surfactants: neutral nonylphenyl polyoxyethylene (NP), anionic sodiumbis (2-ethylhexyl) sulfosuccinate (AOT) and cationic cetyltrimethyl ammonium bromide (CTAB). Fig. 2.13 shows the FTIR peak positions of the azide probe for all three samples, as a function of water content (ω or λ); where,

$$\omega = H_2O \text{ / surfactant} \tag{2.8}$$

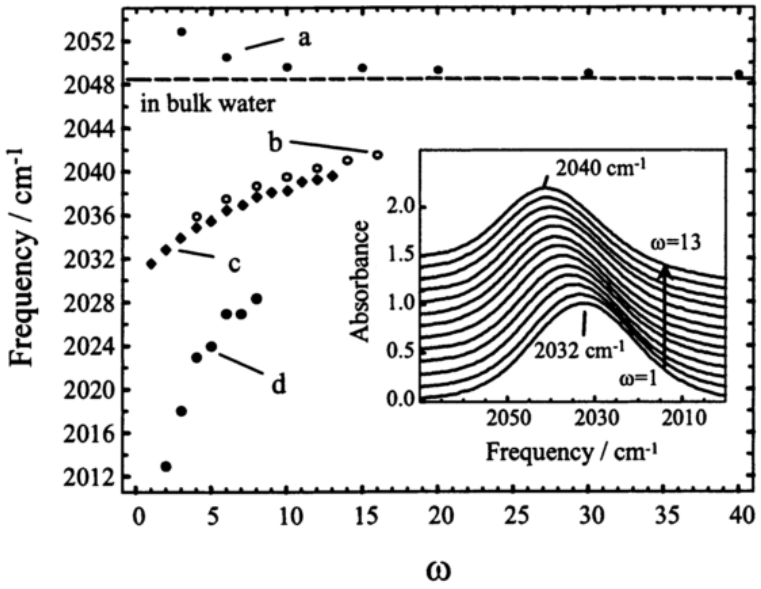

Fig. 2.13 The ν_3 band of N_3^- as a function of ω in RMs formed using (a) AOT (b-c) NP and (d) CTAB surfactants, where the dashed line is the frequency of azide in bulk water.[48]

The frequency of the azide ν_3 band depended on both ω and the surfactant type used to form the RMs, and correlated with the charge of the surfactant. Compared to the frequency of azide in bulk water (2049 cm^{-1}), the band is blue-shifted in anionic AOT, but red-shifted in nonionic NP and cationic CTAB RMs. The shift was related to the charge of the headgroup, as the charge became more positive, the frequency became red-shifted; i.e., ν_3 (AOT) > ν_3 (NP) > ν_3 (CTAB). The researchers also observed that the N_3^- band position for each surfactant tended toward the bulk water value as the hydration number increased. This shift to a bulk-like peak position was interpreted as an increase in the RM pore size. As ω increased, the RMs grew and the fraction of free water increased, so the azide ion was able to penetrate deeper into the interior of the water droplet, reducing the interactions with the surfactant and causing the frequency to blue-shift toward the bulk value. Of note, the azide ν_3 vibrational band shifted continuously as a

function of ω but with little change in the bandwidth, suggesting that the anion does not sample a wide range of water regions.

In summary, most of existing body of knowledge regarding the particular field of the azide anion exists on its interactions with water, and less so on the use of the azide anion as a vibrational probe in solid materials. Till now, no studies have reported the use of an azide probe to measure the hydration behavior in AEM experimental systems. The selection of the azide probe for the purpose of understanding the water dynamics or interactions in AEMs represents an innovative approach. This thesis work was performed with the expectation that the spectral features of the azide probe would render information on the hydrogen bonding environment of water (from the azide peak position) and different water interactions with each QA-PPO.

2.9 References

(1) Kreuer, K.-D. Fuel Cells, Introduction. In *Fuel Cells: Selected Entries from the Encyclopedia of Sustainability Science and Technology*; Kreuer, K.-D., Ed.; Springer New York, 2013; pp 1–7.

(2) Miller, E. L.; Papageorgopoulos, D.; Stetson, N.; Randolph, K.; Peterson, D.; Cierpik-Gold, K.; Wilson, A.; Trejos, V.; Gomez, J. C.; Rustagi, N.; Satyapal, S. U.S. Department of Energy Hydrogen and Fuel Cells Program: Progress, Challenges and Future Directions. *MRS Adv.* **2016**, *1* (42), 2839–2855.

(3) Matthey, J. History of Fuel Cells www.fuelcelltoday.com (accessed Mar 8, 2017).

(4) Scherer, G. G. Fuel Cell Types and Their Electrochemistry. In *Fuel Cells: Selected Entries from the Encyclopedia of Sustainability Science and Technology*; Kreuer, K. D., Ed.; Springer New York, 2013; pp 97–119.

(5) Schulze, M.; Gülzow, E. Degradation of Nickel Anodes in Alkaline Fuel Cells. *J. Power Sources* **2004**, *127* (1–2), 252–263.

(6) Wagner, N.; Schulze, M.; Gülzow, E. Long Term Investigations of Silver Cathodes for Alkaline Fuel Cells. *J. Power Sources* **2004**, *127* (1–2), 264–272.

(7) McLean, G. An Assessment of Alkaline Fuel Cell Technology. *Int. J. Hydrogen Energy* **2002**, *27* (5), 507–526.

(8) Merle, G.; Wessling, M.; Nijmeijer, K. Anion Exchange Membranes for Alkaline Fuel Cells: A Review. *J. Memb. Sci.* **2011**, *377* (1–2), 1–35.

(9) Slade, R. C. T.; Kizewski, J. P.; Poynton, S. D.; Zeng, R.; Varcoe, J. R. Alkaline Membrane Fuel Cells. In *Fuel Cells: Selected Entries from the Encyclopedia of Sustainability Science and Technology*; Kreuer, K.-D., Ed.; Springer New York, 2013; pp 9–29.

(10) Costamagna, P.; Srinivasan, S. Quantum Jumps in the PEMFC Science and Technology from the 1960s to the Year 2000: Part II. Engineering, Technology Development and Application Aspects. *J. Power Sources* **2001**, *102* (1–2), 253–269.

(11) Kreuer, K. D.; Portale, G. A Critical Revision of the Nano-Morphology of Proton

Conducting Ionomers and Polyelectrolytes for Fuel Cell Applications. *Adv. Funct. Mater.* **2013**, *23* (43), 5390–5397.

(12) Paddison, S. J.; Gasteiger, H. A. PEM Fuel Cells, Materials and Design Development Challenges. In *Fuel Cells: Selected Entries from the Encyclopedia of Sustainability Science and Technology*; Kreuer, K. D., Ed.; Springer New York, 2013; pp 341–367.

(13) Varcoe, J. R.; Slade, R. C. T. Prospects for Alkaline Anion-Exchange Membranes in Low Temperature Fuel Cells. *Fuel Cells* **2005**, *5* (2), 187–200.

(14) Couture, G.; Alaaeddine, A.; Boschet, F.; Ameduri, B. Polymeric Materials as Anion-Exchange Membranes for Alkaline Fuel Cells. *Prog. Polym. Sci.* **2011**, *36* (11), 1521–1557.

(15) Jannasch, P.; Weiber, E. A. Configuring Anion-Exchange Membranes for High Conductivity and Alkaline Stability by Using Cationic Polymers with Tailored Side Chains. *Macromol. Chem. Phys.* **2016**, *217* (10), 1108–1118.

(16) Li, X.; Yu, Y.; Meng, Y. Novel Quaternized Poly(arylene Ether Sulfone)/nano-ZrO2 Composite Anion Exchange Membranes for Alkaline Fuel Cells. *ACS Appl. Mater. Interfaces* **2013**, *5* (4), 1414–1422.

(17) Varcoe, J. R.; Atanassov, P.; Dekel, D. R.; Herring, A. M.; Hickner, M. A.; Kohl, P. A.; Kucernak, A. R.; Mustain, W. E.; Nijmeijer, K.; Scott, K.; Xu, T.; Zhuang, L. Anion-Exchange Membranes in Electrochemical Energy Systems. *Energy Environ. Sci.* **2014**, *7*, 3135–3191.

(18) Yan, X.; Gu, S.; He, G.; Wu, X.; Zheng, W.; Ruan, X. Quaternary Phosphonium-Functionalized Poly(ether Ether Ketone) as Highly Conductive and Alkali-Stable Hydroxide Exchange Membrane for Fuel Cells. *J. Memb. Sci.* **2014**, *466*, 220–228.

(19) Wang, G.; Weng, Y.; Zhao, J.; Chu, D.; Xie, D.; Chen, R. Developing a Novel Alkaline Anion Exchange Membrane Derived from Poly(ether-Imide) for Improved Ionic Conductivity. *Polym. Adv. Technol.* **2010**, *21* (8), 554–560.

(20) Li, N.; Yan, T.; Li, Z.; Thurn-Albrecht, T.; Binder, W. H. Comb-Shaped Polymers to Enhance Hydroxide Transport in Anion Exchange Membranes. *Energy Environ. Sci.* **2012**, 7888–7892.

(21) Zhou, J.; Guo, J.; Chu, D.; Chen, R. Impacts of Anion-Exchange-Membranes with Various Ionic Exchange Capacities on the Performance of H2/O2 Fuel Cells. *J. Power Sources* **2012**, *219*, 272–279.

(22) Tomoi, M.; Yamaguchi, K.; Ando, R.; Kantake, Y.; Aosaki, Y.; Kubota, H. Synthesis and Thermal Stability of Novel Anion Exchange Resins with Spacer Chains. *J. Appl. Polym. Sci.* **1997**, *64* (6), 1161–1167.

(23) Hibbs, M. R. Alkaline Stability of Poly(phenylene)-Based Anion Exchange Membranes with Various Cations. *J. Polym. Sci. Part B Polym. Phys.* **2013**, *51* (24), 1736–1742.

(24) Li, N.; Leng, Y.; Hickner, M. A.; Wang, C. Highly Stable, Anion Conductive, Comb-Shaped Copolymers for Alkaline Fuel Cells. *J. Am. Chem. Soc.* **2013**, *135* (27), 10124−10133.

(25) Kushner, D. I.; Zhu, L.; Kusoglu, A.; Hickner, M. A. Side Chain Influence on the Mechanical Properties and Water Uptake of Confined Comb-Shaped Cationic Polymer Thin Films. *Macromol. Chem. Phys.* **2016**, n/a--n/a.

(26) Nakamura, K.; Hatakeyama, T.; Hatakeyama, H. Studies on Bound Water of Cellulose by Differential Scanning Calorimetry. *Text. Res. J.* **1981**, *51* (9), 607–613.

(27) George A. Olah, G. K. Surya Prakash, Árpád Molnár, J. S. *Superacid Chemistry*, 2nd ed.; John Wiley & Sons, Inc., 2009.

(28) Zawodzinski, T. A.; Neeman, M.; Sillerud, L. O.; Gottesfeld, S. Determination of Water Diffusion Coefficients in Perfluorosulfonate Ionomeric Membranes. *J. Phys. Chem.* **1991**, *95*, 6040−6044.

(29) Ohmine, I.; Tanaka, H. Fluctuation, Relaxations, and Hydration in Liquid Water. Hydrogen-Bond Rearrangement Dynamics. *Chem. Rev.* **1993**, *93*, 2545−2566.

(30) Dokter, A. M.; Woutersen, S.; Bakker, H. J. Ultrafast Dynamics of Water in Cationic Micelles. *J. Chem. Phys.* **2007**, *126* (12), 1–10.

(31) Moilanen, D. E.; Piletic, I. R.; Fayer, M. D. Tracking Water's Response to Structural Changes in Nafion Membranes. *J. Phys. Chem. A* **2006**, *110* (29), 9084–9088.

(32) Spry, D. B.; Fayer, M. D. Proton Transfer and Proton Concentrations in Protonated Nafion Fuel Cell Membranes. *J. Phys. Chem. B* **2009**, *113* (30), 10210–10221.

(33) Marino, M. G.; Melchior, J. P.; Wohlfarth, A.; Kreuer, K. D. Hydroxide, Halide and Water Transport in a Model Anion Exchange Membrane. *J. Memb. Sci.* **2014**, *464*, 61–71.

(34) Li, J.; Park, J. K.; Moore, R. B.; Madsen, L. a. Linear Coupling of Alignment with Transport in a Polymer Electrolyte Membrane. *Nat. Mater.* **2011**, *10* (7), 507–511.

(35) Waldron, R. D. Infrared Spectra of HDO in Water and Ionic Solutions. **1957**, *809*.

(36) Falk, M.; Ford, T. Infrared Spectrum and Structure of Liquid Water. *Can. J. Chem* **1966**, *44*, 1699–1707.

(37) Kropman, M. F.; Bakker, H. J. Vibrational Relaxation of Liquid Water in Ionic Solvation Shells. *Chem. Phys. Lett.* **2003**, *370*, 741–746.

(38) Piletic, I. R.; Moilanen, D. E.; Spry, D. B.; Levinger, N. E.; Fayer, M. D. Testing the Core / Shell Model of Nanoconfined Water in Reverse Micelles Using Linear and Nonlinear IR Spectroscopy. **2006**, No. 1, 4985–4999.

(39) Piletic, I. R.; Tan, H.-S.; Fayer, M. D. Dynamics of Nanoscopic Water: Vibrational Echo and Infrared Pump−Probe Studies of Reverse Micelles. *J. Phys. Chem. B* **2005**, *109* (45), 21273–21284.

(40) Black, S. B.; Chang, Y.; Bae, C.; Hickner, M. A. FTIR Characterization of Water-Polymer Interactions in Superacid Polymers. *J. Phys. Chem. B* **2013**, *117* (50), 16266–16274.

(41) Smedley, S. B.; Chang, Y.; Bae, C.; Hickner, M. A. Measuring Water Hydrogen Bonding Distributions in Proton Exchange Membranes Using Linear Fourier Transform Infrared Spectroscopy. *Solid State Ionics* **2015**, *275*, 66–70.

(42) Borgne, C. Le; Illien, B.; Beignon, M.; Chabanel, M.; Spectrochimie, L. De; Sciences, F.; Cedex, N. Ion Association of Alkali and Alkaline Earth Metal Azides in Dimethylsulfoxide . Infrared Spectrometry and Ab Initio Calculations. **1999**, 4701–4706.

(43) Son, H.; Kwon, Y.; Kim, J.; Park, S. Rotational Dynamics of Metal Azide Ion Pairs in Dimethylsulfoxide Solutions. *J. Phys. Chem. B* **2013**, *117* (9), 2748–2756.

(44) Gray, B. Y. P.; Waddington, T. C. Fundamental Vibration Frequencies and Force Constants in the Azide Ion. **1957**.

(45) Sando, G. M.; Dahl, K.; Owrutsky, J. C. Vibrational Spectroscopy and Dynamics of Azide Ion in Ionic Liquid and Dimethyl Sulfoxide Water Mixtures †. **2007**, 4901–4909.

(46) Zhong, Q.; Owrutsky, J. C. Vibrational Energy Relaxation and Reorientation of Azide Ion Pairs in DMSO. *Chem. Phys. Lett.* **2004**, *383* (1–2), 176–180.

(47) Lee, C.; Son, H.; Park, S. Effect of Hydrogen Bonds on the Vibrational Relaxation and Orientational Relaxation Dynamics of HN 3 and N 3 – in Solutions. *J. Phys. Chem. B* **2016**, *120*, 9723–9731.

(48) Zhong, Q.; Steinhurst, D. A.; Carpenter, E. E.; Owrutsky, J. C. Fourier Transform Infrared Spectroscopy of Azide Ion in Reverse Micelles. *Langmuir* **2002**, *18* (20), 7401–7408.

(49) Owrutsky, J. C.; Pomfret, M. B.; Barton, D. J.; Kidwell, D. A.; Owrutsky, J. C.; Pomfret, M. B.; Barton, D. J.; Kidwell, D. A. Fourier Transform Infrared Spectroscopy of Azide and Cyanate Ion Pairs in AOT Reverse Micelles Fourier Transform Infrared Spectroscopy of Azide and Cyanate Ion Pairs in AOT Reverse Micelles. **2008**, *129* (May 2016).

(50) Gai, X. S.; Coutifaris, B. A.; Brewer, S. H.; Fenlon, E. E. A Direct Comparison of Azide and Nitrile Vibrational Probes W. **2011**, 5926–5930.

(51) Lee, H.; Choi, J.; Cho, M. Vibrational Solvatochromism and Electrochromism of Cyanide , Thiocyanate , and Azide Anions in Water W. **2010**, 12658–12669.

(52) Bales, B. L.; Zana, R. Characterization of Micelles of Quaternary Ammonium Surfactants as Reaction Media I: Dodeclytrimethylammonium Bromide and Chloride. *J. Phys. Chem. B* **2002**, *106* (8), 1926–1939.

(53) Chingakule, D. D. K.; Gans, P.; Gill, J. B.; Longdon, P. J. Spectrochemistry of Solutions, Part 23. Changes of Enthalpy and Entropy in the Formation of Contact Ion Pairs: A Vibrational Spectroscopic Appraisal Using Thiocyanate and Azide Solutions. *Monatshefte fur Chemie / Chem. Mon.* **1992**, *123* (6), 521–535.

(54) Sando, G. M.; Dahl, K.; Zhong, Q.; Owrutsky, J. C. Vibrational Relaxation of

Azide in Formamide Reverse Micelles. *J. Phys. Chem. A* **2005**, *109* (26), 5788–5792.

(55) Zhong, Q.; Baronavski, A. P.; Owrutsky, J. C. Vibrational Energy Relaxation of Aqueous Azide Ion Confined in Reverse Micelles. *J. Chem. Phys.* **2003**, *118* (15).

(56) Owrutsky, J. C.; Pomfret, M. B.; Barton, D. J.; Kidwell, D. A. Fourier Transform Infrared Spectroscopy of Azide and Cyanate Ion Pairs in AOT Reverse Micelles. *J. Chem. Phys.* **2008**, *129* (2).

Chapter 3

Material and Methods

3.1 Introduction

The thesis work presented here is subdivided into two parts: solution studies of the azide probe and QA-PPO polymer studies. Using a study characterizing the dynamics of azide in DMSO-water mixtures[1] as a guide, the solutions studies intended to pursue further studies with different solvent mixtures/environments to serve as a foundation for its use as a vibrational probe. The polymer studies were performed to study the different QA-PPOs and measure the hydration behavior in these AEM experimental systems.

3.2 Solution Studies

Sodium azide (NaN_3, 99%, Sigma Aldrich) and tetrabutylammonium azide ($TBAN_3$, 97%, Sigma Aldritch) were used as received. Initially, a series of spectra for NaN_3 in solutions were obtained, but the work later used $TBAN_3$ to simplify the spectral fitting (see Appendix A). Furthermore, $TBAN_3$ was soluble in all solvents selected for the solutions studies. Dimethyl sulfoxide (DMSO, ACS grade, Macron) was used because it is a polar aprotic solvent, miscible in water and with a dielectric constant (ε) of 46.7. Tetrahydrofuran (THF, ACS grade, VWR) was used because it is also a polar aprotic solvent and miscible in water, but with a lower ε of 7.58. Methanol (MeOH, ACS grade,

VWR) was used because it is a polar protic solvent with a ε of 32.7. Chloroform (99%, Sigma Aldritch) was used because it is a non-polar solvent, immiscible in water and with a ε of 4.81. The water utilized was of high-purity, obtained from a lab water system (Marlo, Inc.).

From these solvents, the following mixtures were selected for the studies with $TBAN_3$: DMSO-H_2O, THF-H_2O, Chloroform-MeOH, and DMSO-Chloroform. All mixtures were prepared from stock solution of 0.05M $TBAN_3$ to ensure constant solution concentration during the experiment and in various mole fraction mixtures. In DMSO-H_2O and THF-H_2O mixtures, the molar fraction of H_2O was calculated (X_W). In Chloroform-Methanol mixtures, the molar fraction of methanol was calculated (X_M). In DMSO-Chloroform mixtures, the molar fraction of chloroform was calculated (X_C). Solvents blank solutions (without $TBAN_3$) were also prepared for measuring spectra to use for background subtraction.

Steady-state spectra were collected on a VERTEX 70 (Bruker Corporation) Fourier transform infrared (FTIR) spectrometer using the Horizon horizontal ATR accessory (Harrick) with a 4 cm^{-1} resolution on a zinc selenide (ZnSe) crystal. The spectra were baseline corrected and extracted to Origin 8.0 software (OriginLabs, Northhampton, MA) to be analyzed and prepared on a graph. The steady-state spectra were fitted with a function where each band is a sum of a Gaussian and Lorenztian functions that were constrained to have the same peak position and width on OPUS software (Bruker Corporation).

3.3 Polymer Studies

3.3.1 Quaternary Ammonium Anion Exchange Membranes

A series of quaternized ammonium comb-shaped polymers based on poly(2,6-dimethyl-1,4- phenylene oxide) (QA-PPO) were synthesized by Liang Zhu from the Michael A. Hickner Research Group using the procedure discussed in detail elsewhere.[2,3] Commercially available PPO was used as the backbone material; their methyl groups were brominated, using *N*-bromosuccinimide (NBS) and azobisisobutyronitrile (AIBN) then dissolved in *N*-methylpyrrolidone (NMP) to form brominated PPO. Afterwards, the comb-shaped ionomers were achieved by the Menshutkin reaction. Three comb-shaped QA-PPO polymers were synthesized with a pendant n-alkyl side chain; consisting of six, ten and sixteen carbons on the side chain and referred to as C6D40, C10D40, and C16D40, where C***x*** represents the total number of carbons on the side chain and D40 refers to the degree of bromination, where there are 0.4 bromomethyl groups per PPO repeat unit as shown in Fig. 3.1. A control polymer was also synthesized, with the same degree of bromination but contained no pendant alkyl side chain, referred to as benzyltrimethyl ammonium QA-PPO (BTMA40).

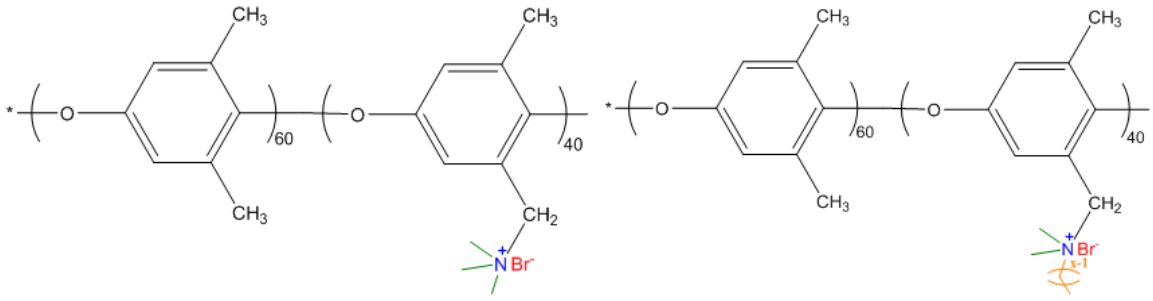

Fig. 3.1 Chemical structure of the comb-shaped QA-PPO, where x = number of carbons in the n-alkyl side chain.

3.3.2 FTIR sample preparation and experimental procedures

A thin (~10 μm) film of each polymer in bromide form was drop-cast onto a germanium (Ge) trapezoidal crystal from a 10 wt % solution in N-methyl-2-pyrrolidone (NMP). The films were then dried in a vacuum oven at 80 °C for 24h. The resultant film was immersed for only 5 min, to avoid degradation (see Appendix C), with an azide sodium solution (0.05M NaN_3) to incorporate the azide ions into the polymer network, as shown in the schematic in Fig 3.2.

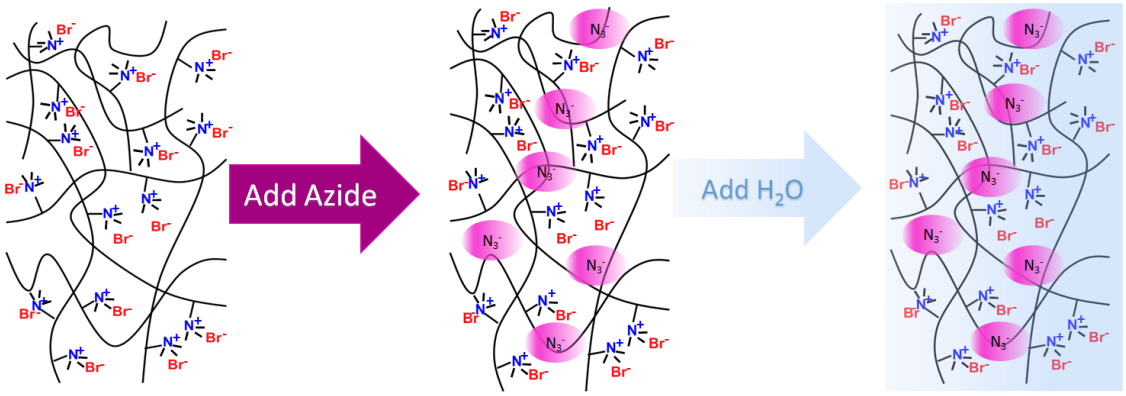

Fig, 3.2 Schematic of the incorporation of azides ions into the polymer network and soaking procedure.

The samples were then placed on a Horizon ATR accessory (Harrick) and sealed with the flow cell for horizontal attenuated total reflectance (HATR), as seen in Fig. 3.3. The thin films were exposed to a controlled relative humidity (RH) at 0%, 25%, 50%, 75% and 90% RH to measure the spectral response of the azide peak at those different RH environments inside the flow cell. To clarify, first the polymer samples were kept for more than 24 hours at 0% RH to ensure they were fully dry, and then throughout the *in-situ* monitoring of the hydration experiment, each RH step was left for at least 30 minutes. All spectra were recorded, with a 4 cm^{-1} resolution, at 200 scans, every 5min on

the VERTEX 70 (Bruker Corporation) FTIR spectrometer equipped with a liquid nitrogen cooled wide band Mercury-Cadmium-Telluride (MCT) detector at an ambient temperature of approximately 22 °C. Spectra were two point baselined corrected and extracted to Origin 8.0 software (OriginLabs, Northhampton, MA) to be presented in graph format. The spectra were then fitted using a Levenberg-Marquardt algorithm[4,5] with mixed Lorenztian and Gaussian peak shape functions that were constrained to have the same peak position and shape on OPUS software (Bruker Corporation).

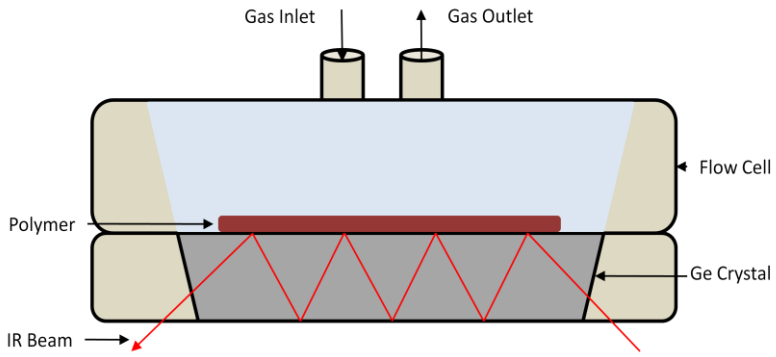

Fig 3.3 Schematic of ATR flow cell used to introduce humidified air in the chamber containing the polymer sample while doing *in-situ* measurements.

Each RH corresponded to a different hydration number depending on the polymer being studied.[5] The hydration number was calculated by:

$$\lambda = \left(\frac{m_{RH} - m_{dry}}{m_{dry}}\right)\left(\frac{1000}{M_{H_2O} * IEC}\right) \tag{3.1}$$

where, m_{RH} is the samples' mass at a given RH, m_{dry} is the mass of the dry sample, M_{H2O} is the molar mass of water (i.e. 18.02 g). These masses were measured using a TA instrument Q5000SA water vapor sorption microbalance. The ion exchange capacity (IEC) varies for each polymer; BTMA has a theoretical IEC of 2.66 meq. g^{-1} (i.e.

milliequivalents of ions per gram of polymer), C6 has an IEC of 2.2 meq. g^{-1}, C10 has an IEC of 1.97 meq. g^{-1}, and C16 has an IEC of 1.7 meq. g^{-1}.[3,4]

The RH was generated, as seen in Fig 3.4, by mixing humidified air at dew point with dry air at ambient temperature of approximately 22 °C. Humid air at dew point was produced by sparging air in a water reservoir held in a heated water bath at 30 °C. The total flow rate of dry air supplied from a gas generator was regulated at a constant flow rate using electronic mass flow controllers (FMA 5514, Omega Engineering, Stamford, CT) and a custom LabVIEW (National Instruments Corp., Austin, TX) program. Humidity and temperature were measured and recorded using an Omega HX15-W RH sensor (Omega Engineering, Stamford, CT).

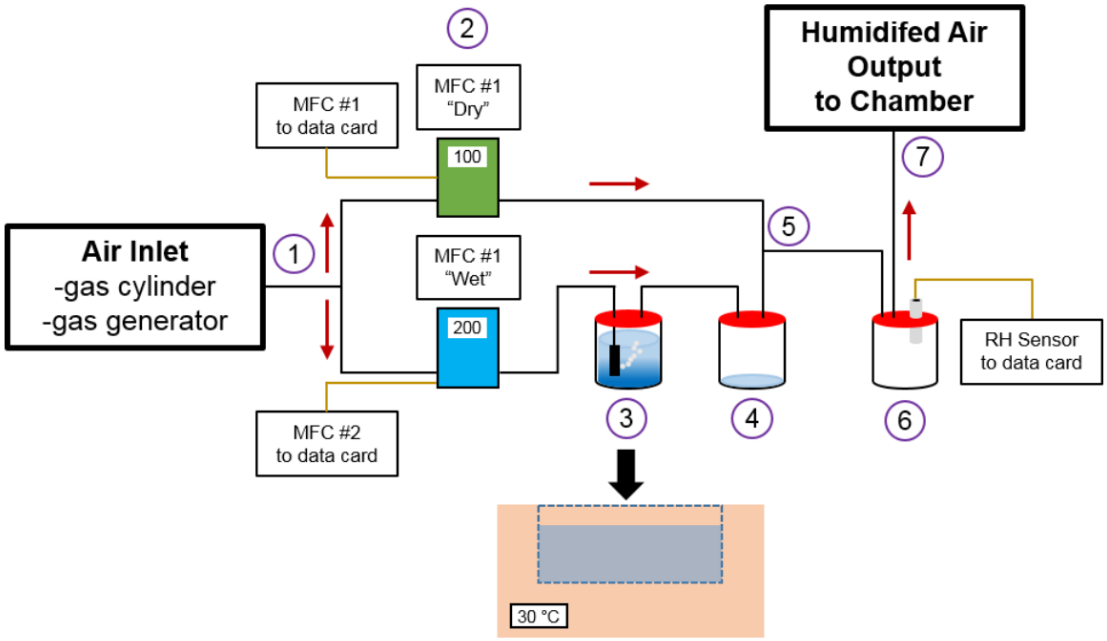

Fig. 3.4 Schematic of the RH generation system used in the experiments, includes: (1) air inlet that is divided into two lines (2) mass flow controllers control the ratio of air that flows through the wet and dry stream, (3) dry air is directed into a bubbler held at a temperature of 30 °C to produce air at dew point, (4) saturated water vapor is condensed in a jar, (5) wet and dry air streams are recombined, (6) the humidified air is directed to the RH sensor, and (7) the humidified air is directed to the sample chamber.[4]

3.4 References

(1) Sando, G. M.; Dahl, K.; Owrutsky, J. C. Vibrational Spectroscopy and Dynamics of Azide Ion in Ionic Liquid and Dimethyl Sulfoxide Water Mixtures †. **2007**, 4901–4909.

(2) Li, N.; Yan, T.; Li, Z.; Thurn-Albrecht, T.; Binder, W. H. Comb-Shaped Polymers to Enhance Hydroxide Transport in Anion Exchange Membranes. *Energy Environ. Sci.* **2012**, 7888–7892.

(3) Li, N.; Leng, Y.; Hickner, M. A.; Wang, C. Highly Stable, Anion Conductive, Comb-Shaped Copolymers for Alkaline Fuel Cells. *J. Am. Chem. Soc.* **2013**, *135* (27), 10124−10133.

(4) Donald W. Marquard. An algorithm for least-squares estimation of nonlinear parameters. *J. Soc. Indust. Appl. Math* **1963**, *11* (2).

(5) More, J. J. The Levenberg-Marquardt Algorithm: Implementation and Theory.

(6) Kushner, D. I.; Zhu, L.; Kusoglu, A.; Hickner, M. A. Side Chain Influence on the Mechanical Properties and Water Uptake of Confined Comb-Shaped Cationic Polymer Thin Films. *Macromol. Chem. Phys.* **2016**.

Chapter 4

Results and Discussion

4.1 Introduction

Taking into consideration that the main goal of this thesis was to measure the hydration of cationic polymers with Fourier transform infrared spectroscopy using the azide anion as a vibrational probe, the work was subdivided into two parts: solution studies of the azide probe and polymer studies with membranes imbibed with azide probes. The solutions studies were deemed important to understand the interaction of the azide anion in different solvent mixtures/environments as a foundation for its use as a vibrational probe to measure the hydration behavior in AEMs. Studies were conducted on four sets of mixtures, dimethyl sulfoxide (DMSO)-H_2O, tetrahydrofuran (THF)-H_2O, chloroform-methanol (MeOH), and DMSO-chloroform; these results are presented first. The polymer studies were conducted on a series of QA-PPOs and the results are presented after the solution studies.

4.2 Azide in Different Solutions

A vibrational spectroscopy study characterizing the dynamics of the azide ion in DMSO-water mixtures[1] served as a guide to further pursue studies with $TBAN_3$ in different solvent environments. Studies were initiated with sodium azide (NaN_3);

however, the appearance of an ion-pair band complicated the spectral peak fitting (see Appendix A); upon switching to $TBAN_3$, the ion-pair band was removed and it simplified the spectral fitting. Regarding the studies with $TBAN_3$, they will be presented in sequence. First, DMSO, which has a dielectric constant (ε) of 46.7, was studied in mixtures with water, and then compared to the previously published work[1]. Second, THF, which has a ε of 7.58, is miscible with water and dissolves $TBAN_3$, was included as a polar aprotic solvent and studied in water mixtures. Third, chloroform, which has a low ε of 4.81, is immiscible with water but dissolves $TBAN_3$, was included as a non-polar solvent and studied in mixtures with MeOH, a polar protic solvent. Fourth, chloroform was also studied in mixtures with DMSO, a polar aprotic solvent with a ε of 46.7. The results of these four sets of solutions studies are presented in detail below.

4.2.1 Azide in DMSO – H_2O mixtures

The FTIR spectra for $TBAN_3$ (0.05M) in mixtures of DMSO – H_2O from 0 to 1 mole fraction of water (X_W), are presented in Fig. 4.1. In pure DMSO (X_W = 0), the strongest band is the asymmetric stretching (υ_3) frequency of the azide, which appeared at 2000 cm^{-1}, designated as the "dry" band. Another weaker band appeared at a lower wavenumber of 1985 cm^{-1}. When water was added (X_W = 0.02), one band appeared at 2009 cm^{-1}, designated as the "wet" band. These "dry" and "wet" bands are thought to arise from the same asymmetric stretch of the azides' resonance structures, as will be discussed below. At X_W = 0.06 the "wet" band gains absorbance while the "dry" band decreases absorbance; as the X_W increased the "wet" band continues to blueshift, while

the "dry" band does not shift much. When enough water is added to reach X_W = 0.25 only a single band is observed at 2011 cm^{-1}. The band continues to blueshift to higher frequency with increasing X_W until it reaches the bulk water (X_W = 1) value at 2047 cm^{-1}. The spectra for the $TBAN_3$ in DMSO – H_2O mixtures were fitted using the appropriate number of mixed Lorentzian/Gaussian functions and the results are presented in Table 4.1. The entire set of parameters from the analysis is available in Appendix B (Table B0.1).

When comparing the data obtained here with the previously published vibrational spectroscopy study characterizing the azide ion in DMSO-water mixtures[1], the data showed similar results. Slight differences could be attributed to the methodology of obtaining the spectra; Sando, et al.[1] conducted the experiments with a Harrick transmission cell, while we used the HATR accessory to obtain the spectra. Overall, the spectra appeared similar, with the same wavenumber, as the previously published results.[1] The additional bands appearing at an approximate 1985 cm^{-1} value, from X_W = 0 to X_W = 0.15, were also described by Sando, et al.[1], where they designated this band as the bending "hot" band, due to thermal population of the bending state (υ_2), i.e., the $\upsilon_3 + \upsilon_2 - \upsilon_2$ band. The researchers explained how their DMSO-water mixtures exhibited an inhomogeneous pattern at low mole fractions, becoming apparent when two bands were resolved in the spectra; as found in our results. They also described how the "wet" band appeared to the blue side of the DMSO frequency when water was added, and as the amount of water increased, the "wet" band shifted blue and gained strength; indicating that as more water was added, a higher fraction of anions had water penetrating into the first solvent shell. This same phenomenon of probe frequency dependence was observed

in our study, as described above. Sando, et al.[1] interpreted this probe frequency dependence to be a signature finding of a mixed solvation environment.

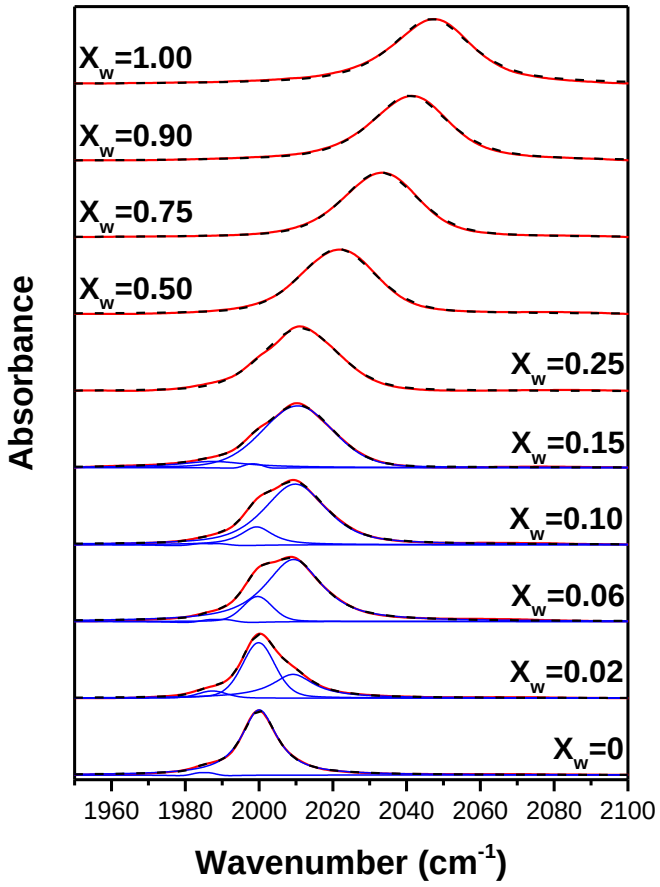

Fig. 4.1 FTIR spectra of $TBAN_3$ in various mole fraction mixtures of water and DMSO. The red solid line represents the experimental spectrum. The black dashed line is the total fit. The blue lines are the individual components for the bands.

Table 4.1 Spectroscopic parameters of $TBAN_3$ in DMSO-H_2O mixtures.

Mole Fraction	Wavenumber (cm^{-1})		
	"Hot" band	"Dry" band	"Wet" band
0	1985	2000	
0.02	1987	2000	2009
0.06	1989	1999	2009
0.10	1987	1999	2010
0.15	1987	1998	2010
0.25			2011
0.50			2021
0.75			2033
0.90			2041
1			2047

It has been reported that azides have three different resonance structures, as depicted in Fig 4.2. In gas phase, azides exhibit a band at a lower wavenumber (1986 cm^{-1}) because the symmetric double-bond structure ($^{-}N=N^{+}=N^{-}$) is preferred. In liquid phase, the asymmetric single-/triple-bond structure ($N\equiv N^{+}-N^{2-}$) is preferred and exhibits a band at a higher wavenumber (2000 cm^{-1}).[2,3] *Abinitio* calculations of azide in water clusters demonstrated that solvent distributions around the azides favor asymmetric bond lengths, leading to the higher solvated frequency.[4] The blueshift in H_2O suggests that the asymmetric N–N≡N structure is stabilized by the solvent charges, i.e. water and azides form charge redistributions. The calculations mentioned also indicated that charge transfer within water occurred, therefore, the azide charge ranged from -0.86 to -1.02 depending on the water cluster size and geometry.[5,4] According to Lee et al,[6] a ratio of seven water molecules to one molecule of azide accounted for 45% of the equilibrium structure distribution while a ratio of six and eight water molecules to one azide accounted for 31% and 21%, respectively.

In the following, we will correlate the discussed azide resonance structure with our findings. In H_2O, the azide ion is mostly stabilized in a triple bond resonance form, displaying a wavenumber at 2047 cm^{-1}. Hypothetically, the larger blueshift (61 cm^{-1}) relative to the azide peak position at the gas phase (1986 cm^{-1}) represents an increased tightening of the triple bond state. In DMSO, the azide ion is in a less stable triple bond resonance form, displaying a wavenumber at 2000 cm^{-1} and having a smaller blueshift (14 cm^{-1}) relative to the azide peak position at the gas phase. Finally, in chloroform, azides exhibit an intermediate blueshift.

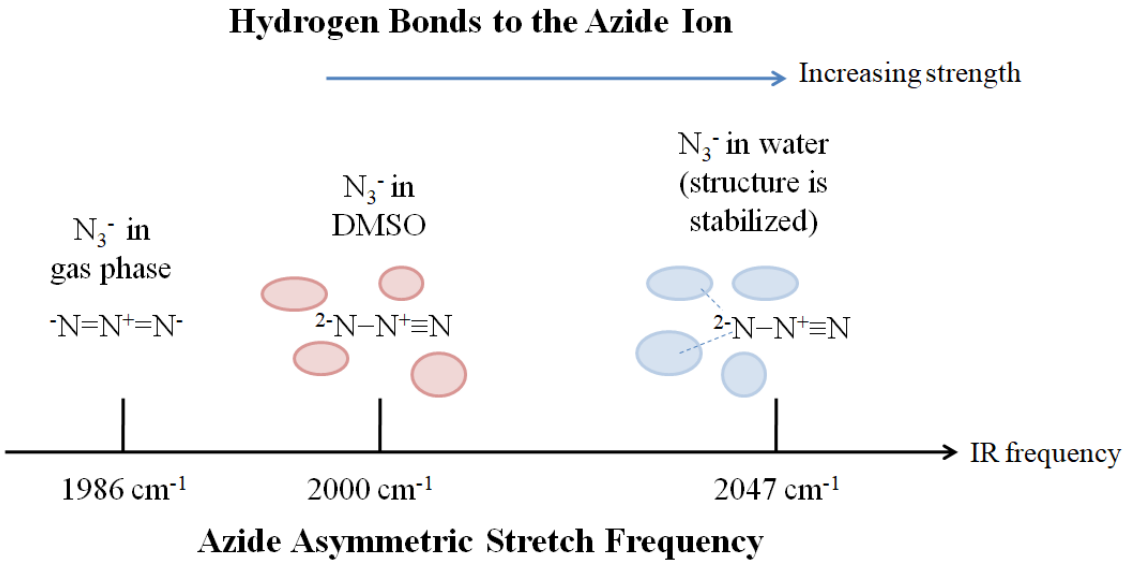

Fig. 4.2 Schematic of the azide asymmetric stretch frequency in different environments. Red ovals represent DMSO molecules; blue ovals represent water molecules and dash lines represent hydrogen bonding.[2,3]

4.2.2 Azide in THF – H_2O mixtures

The FTIR spectra for $TBAN_3$ (0.05M) in mixtures of THF – H_2O from 0 to 1 mole fraction of water (X_W), are presented in Fig. 4.3. In pure THF ($X_W = 0$), the strongest band is the antisymmetric stretching (υ_3) band of the azide, which appeared at 2004 cm^{-1}. Another weaker band appeared at a lower wavenumber of 1993 cm^{-1}. When water was added ($X_W = 0.02$), two bands appeared, one at 2018 cm^{-1} and the other at 2027 cm^{-1}. At $X_W = 0.06$ a single band provided an acceptable fit; as the X_W increased the azide band continued to blueshift until it reached the bulk water ($X_W = 1$) value at 2047 cm^{-1}. The spectra for the $TBAN_3$ in THF – H_2O mixtures were fitted using the appropriate number of mixed Lorentzian/Gaussian functions and the results are presented in Table 4.2. The entire set of parameters from the analysis is available in Appendix B (Table B0.2).

The absorption profile of the azide at $X_W = 0$, or pure THF, in Fig 4.3 shows the maximum absorbance at 2004 cm^{-1} and an unexpected band at 1993 cm^{-1}, which is an added complexity that has not been described in THF solutions previously. Although unexpected, a similar complexity has been described in a few studies of the azide absorbance band of aryl azides, such as 3-azidopyridine, in biomolecular studies.[2–4] The observed complexity of the tetrabutyl ammonium azide asymmetric stretch in THF may be the result of either multiple conformations of $TBAN_3$ in THF, or Fermi resonance involving the azide asymmetric stretch and a normally forbidden combination or overtone band.[4] We interpret that the 2004 cm^{-1} band is the azide asymmetric stretch and assume that the secondary band at 1993 cm^{-1} is the normally forbidden combination or overtone

band participating in the Fermi resonance; however, further research is required to elucidate this finding.

Our data for the X_W = 0.02 sample reflects a much different behavior than what has been described in DMSO – water mixtures[1]. Of the two bands, the lower frequency band (2018 cm^{-1}) is interpreted to correspond to the material not interacting with water, so this band was designated as the "dry" band. The second band at 2027 cm^{-1} is interpreted to correspond to the azide anion interacting with water, so it was designated the "wet" band. A noticeable finding is the drastic shift from 2004 cm^{-1} to 2018 cm^{-1} at X_W = 0.02, representing a 14 cm^{-1} difference. One explanation for this shift could be that the addition of a small amount of water caused a drastic change in the environment; thus, significantly altering the interactions of THF with azide and provoking a significant shift. This drastic change at low volume fractions of water contrasts with the evolution of the "wet" and "dry" bands seen in the previously published DMSO–water mixture study[1], where gradual changes of a growing, blueshifting "wet" band and a diminishing, weakly shifting "dry" band are seen from X_W = 0.02 to X_W = 0.25.

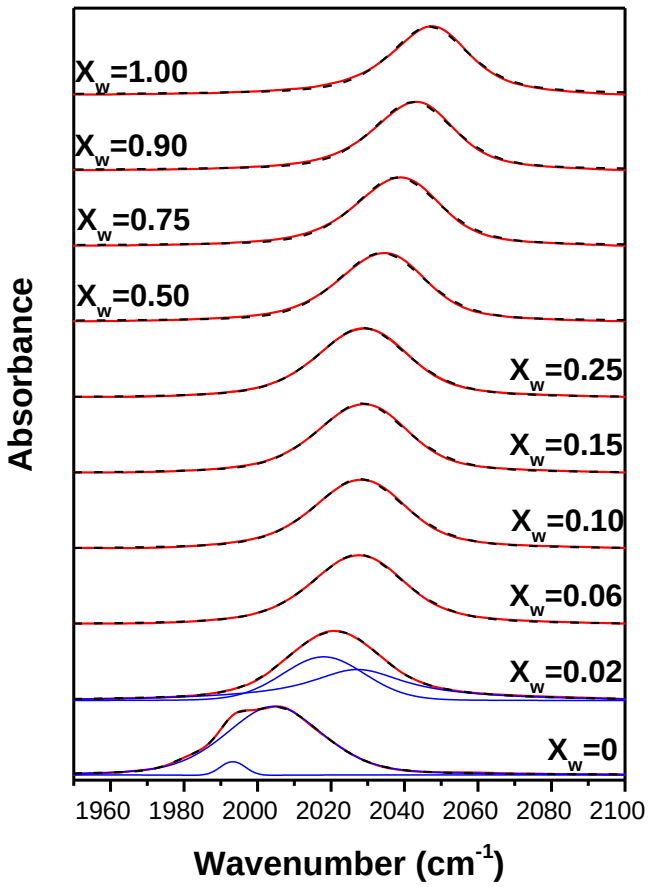

Fig. 4.3 FTIR spectra of $TBAN_3$ in various mole fraction mixtures of water and THF. The red solid line represents the experimental spectrum. The black dashed line is the total fit. The blue lines are the individual components for the bands.

Table 4.2 Spectroscopic parameters of $TBAN_3$ in THF-H_2O mixtures.

Mole Fraction	Wavenumber (cm^{-1})		
	Unknown band	Dry band	Solution band
0	1993	2004	
0.02		2018	2027
0.06			2027
0.10			2028
0.15			2028
0.25			2029
0.50			2034
0.75			2038
0.90			2042
1			2047

4.2.3 Azide in Chloroform – MeOH mixtures

The FTIR spectra for $TBAN_3$ (0.05M) in mixtures of chloroform – methanol from 0 to 1 mole fraction of methanol (X_M) are presented in Fig. 4.4. In a solution of pure chloroform ($X_M = 0$), a single band provided an acceptable fit at 2012 cm^{-1}. When water was added ($X_M = 0.02$), the band blueshifted considerably to 2023 cm^{-1}. In addition to the shifting, the width of the asymmetric stretching mode broadened (~8 cm^{-1}, from a FWHM of 17.9 cm^{-1} to 25.9 cm^{-1}) as compared to the band displayed by azide in pure chloroform. As the X_M increased, the azide band continued to blueshift until it reached the pure methanol ($X_M = 1$) value at 2043 cm^{-1}. The spectra for the $TBAN_3$ in chloroform – methanol mixtures were fitted using the appropriate number of mixed Lorentzian/Gaussian functions and the results are presented in Table 4.3. The entire set of parameters from the analysis is available in Appendix B (Table B0.3).

The observed broadening of the width of the asymmetric stretching band upon introducing methanol, as compared to pure chloroform can be explained by the azide's solvatochromic effect. This solvatochromic effect, refers to the capacity of azide to vary its position, intensity and shape depending upon its immediate environment.[5] Chloroform is a non-polar solvent and methanol is a polar protic solvent; hence, a change in the solvent polarity or environment is introduced as methanol is added to the mixture, which is reflected in the resulting spectra.

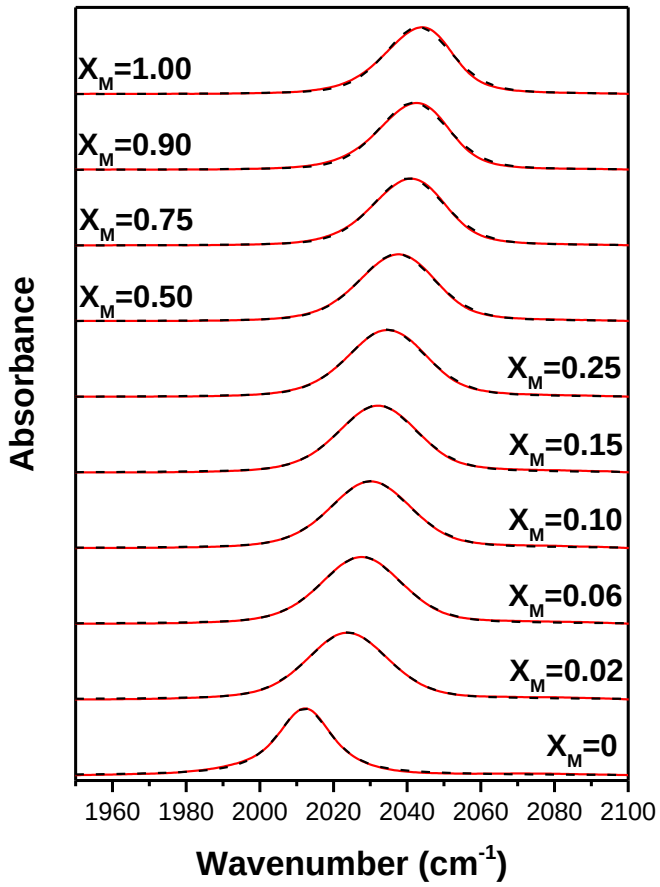

Fig. 4.4 FTIR spectra of $TBAN_3$ in various mole fraction mixtures of chloroform and methanol. The red solid line represents the experimental spectrum. The black dashed line is the total fit.

Table 4.3 Spectroscopic parameters of $TBAN_3$ in Chloroform-MeOH mixtures.

Mole Fraction	Wavenumber (cm^{-1})
	Azide band
0	2012
0.02	2024
0.06	2028
0.10	2030
0.15	2032
0.25	2034
0.50	2037
0.75	2040
0.90	2042
1	2043

4.2.4 Azide in DMSO – Chloroform mixtures

The FTIR spectra for $TBAN_3$ (0.05M) in mixtures of DMSO - chloroform from 0 to 1 mole fraction of chloroform (X_C) are presented in Fig. 4.5. In a solution of pure DMSO (X_C = 0), two bands were fitted at 2000 cm^{-1} and at 1985 cm^{-1}, as previously discussed in section 4.2.1. When chloroform was added (X_C = 0.02), the band blueshifts slightly to 2001 cm^{-1}. As the X_C increased, the azide band continued to blueshift until it reached the pure Chloroform (X_C = 1) value at 2012 cm^{-1}. Additional weaker bands appeared at approximately 1985 cm^{-1}, from the mixture of pure DMSO (X_C = 0) up to X_C = 0.25, which was designated as the "hot" band (discussed in section 4.2.1). The remaining mole fractions (X_C = 0.50 to X_C = 1.00) were able to be fitted with a single band. The spectra for the $TBAN_3$ in chloroform – DMSO mixtures were fitted using the appropriate number of mixed Lorentzian/Gaussian functions and the results are presented in Table 4.4. The entire set of parameters from the analysis is available in Appendix B (Table B0.4).

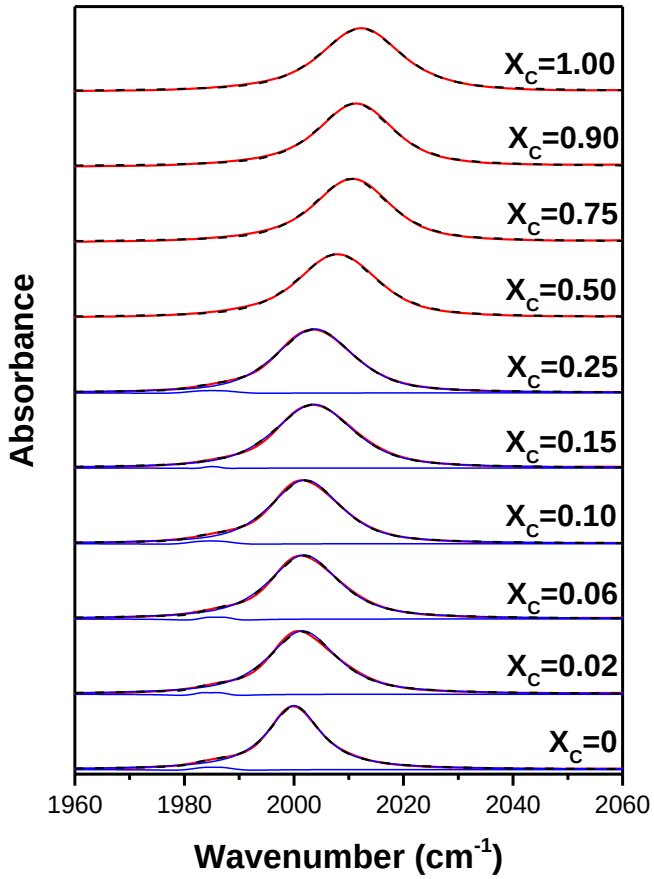

Fig. 4.5 FTIR spectra of $TBAN_3$ in various mole fraction mixtures of DMSO and chloroform. The red solid line represents the experimental spectrum. The black dashed line is the total fit.

Table 4.4 Spectroscopic parameters of $TBAN_3$ in DMSO-Chloroform mixtures.

Mole Fraction	Wavenumber (cm^{-1})	
	Azide band	Hot band
0	2000	1985
0.02	2001	1985
0.06	2002	1986
0.10	2002	1985
0.15	2004	1985
0.25	2004	1985
0.50	2008	
0.75	2010	
0.90	2011	
1	2012	

4.2.5 Summary of Azide - Solvent mixtures

All the data gathered from the work performed on azide solutions are summarized in Fig. 4.6. Bear in mind, the results for DMSO and THF–water mixtures only display the data from the "wet" band, which is the azide interacting with the water molecules. Overall, it is evident that all mixtures behave similarly, exhibiting a blueshifting pattern. However, they each exhibit different wavenumber positions, which are directly related to the characteristics of the solvents. Both the THF and DMSO mixtures with water have a similar trend in displaying a smaller shift at the beginning (i.e. lower mole fractions) and then larger shifts at higher mole fractions. But their intermediate behavior shows some difference, which can be explained, in part, due to the fact that DMSO has a higher dielectric constant (so, it mixes well with water) and THF has a lower dielectric constant (so, it does not mix well and forms clusters of water). Regarding the FTIR spectra of $TBAN_3$ in pure THF and DMSO solutions (seen more clearly in Appendix A), THF demonstrated a complex absorption profile that still requires elucidation, while DMSO demonstrated a less complex absorption profile that has been described above (section 4.2.1) and by Sando et al[1], consisting of the appearance of a weak band shoulder on the low-frequency side of the dominant band, at ~1987 cm^{-1}, designated as the "hot" band. Of note, in our study the band appears at ~1985 cm^{-1}.

Fig. 4.6 also demonstrates how hydrogen bonding plays a dominant role rather than the dielectric constant, making the single/triple-bond structure more stable, relative to the peak position of the azide asymmetric stretch band.[6] When the solvents are added, the band blueshifts to a higher wavenumber, according to the ability of each solvent to

form hydrogen bonds. Taking into account the findings in this study, the solvents can be divided into separate groups; one, where solvents interact strongly with the azide, such as H_2O and MeOH; two, where solvents interact weakly with the azide such as DMSO and THF; and three, where solvents show an intermediate interaction with the azide such as Chloroform. For H_2O and MeOH (polar protic solvents), the azide ion acts as a hydrogen bond accepter. For THF and DMSO, both act as poor hydrogen bond donors. Finally, chloroform, a non-polar solvent, has three electron-withdrawing groups (Cl) attached directly to the C-H group, which makes this bond polar and enables it to act as a stronger hydrogen bond donor than THF and DMSO.[9]

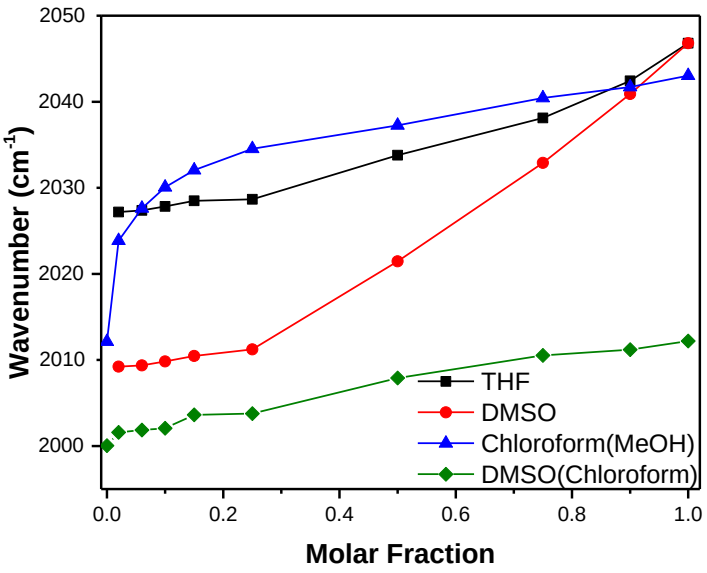

Fig. 4.6 Representative summary of the azide solutions work done with DMSO-H_2O, THF-H_2O, Chloroform-Methanol and DMSO-Chloroform mixtures expressed as wavelength position vs. molar fraction.

4.3 QA-PPO and Azide

After the QA-PPO polymer samples were cast they were immersed for 5 min, to avoid degradation (see Appendix C), in a 0.05M solution of NaN_3 in order to successfully imbibe the azide into the polymer films. The FTIR spectra of the azide asymmetric stretch bands for the different QA-PPO samples are shown at Fig. 4.7, where the wavenumber of the azide band has been expressed as a function of hydration number (λ). Noticeably, all of the QA-PPO polymers displayed a gradual blueshifting of the azide asymmetric stretch with increasing λ, consistent with the known solvatochromic effect of azides.[5] Furthermore, the asymmetric stretch also showed decreasing absorbance with increasing λ. BTMA is observed to reach a higher λ, while C16 had the lowest λ, most likely due to the hydrophobicity of the C16 tether. Moreover, BTMA had the largest wavenumber shift when compared to the comb-shaped polymers; the azide resonance in BTMA started at approximately 2000 cm^{-1} at λ=0 and shifted to approximately 2026 cm^{-1} at λ=4.32, while the smallest shift was observed for azide in C16, from ~2000 cm^{-1} at λ=0 to 2020 cm^{-1} at λ=2.35; the other comb-shaped polymers fell in-between these two parameters. The blueshift of the azide wavenumber is interpreted as an increase towards bulk water behavior with increasing λ, concurring with the studies by Zhong, et al[10] performed on reverse micelles.

An interesting find is that the non-interacting azide, or "dry" azide at λ=0, exhibited a peak at 2000 cm^{-1}, indicating negligible interactions between the azide anion and the polymer. This is consistent with our similar finding of a peak at 2000cm^{-1} with pure DMSO (X_W = 0), described above at 4.2.1 within the solution studies. At low λ,

water within the QA-PPO membranes will interact with both the azide ion and the bromide counter ion at the QA/water interface. As λ increases, the hydration sphere of the bromide counter ion is filled and its influence on hydrogen bonding becomes progressively weaker. The net result is that the azide probe experiences a hydrogen-bonding environment closer to that of bulk water behavior, as λ increases.

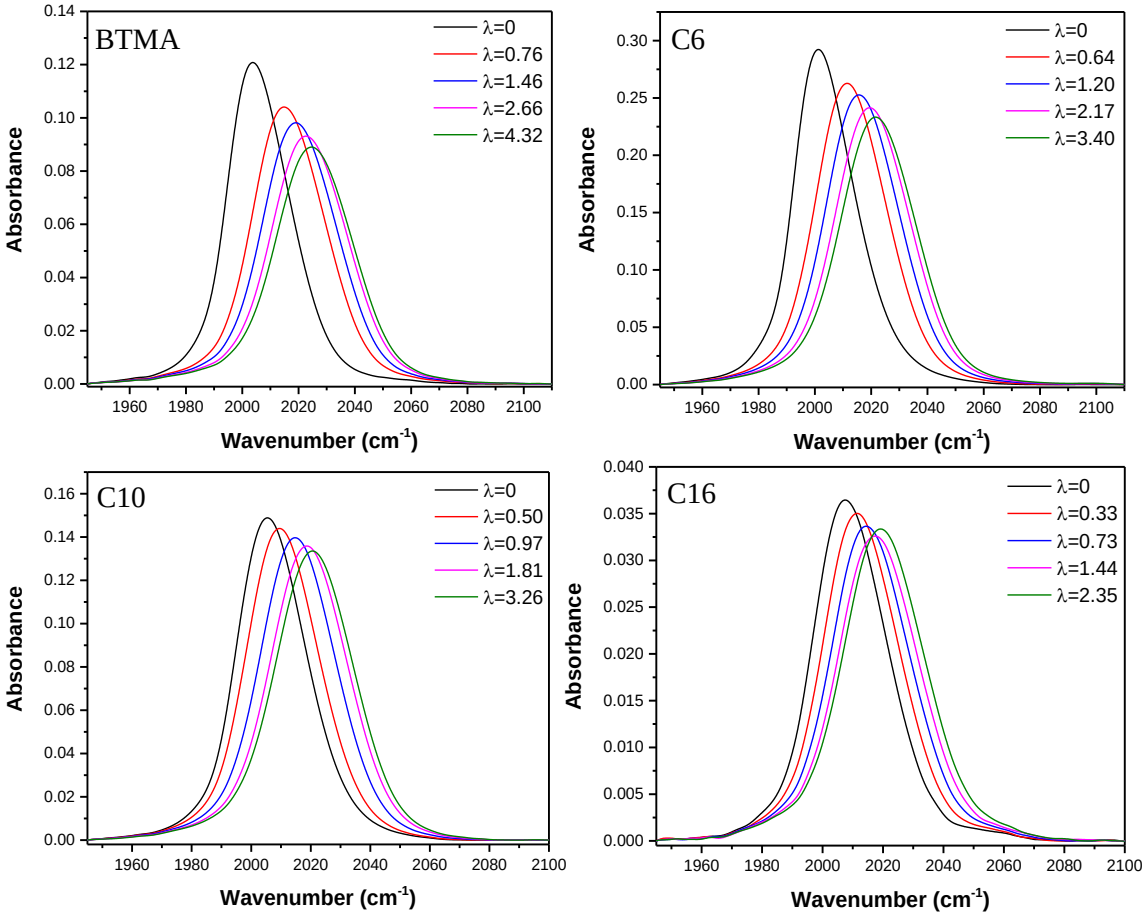

Fig. 4.7 The azide asymmetric stretch in the different comb-shaped polymers.

After performing the experiment on three different samples, the Fig. 4.8 represents a summary (an average of all values obtained after each experimental set) of the azide band position, taking into account both relative humidity (RH) and λ for all QA-

PPO samples. In Fig. 4.8 (a), all the polymers are expressed with RH, ranging from 0%, 25%, 50%, 75% to 90% RH. Here, it is more noticeable how the polymers with alkyl chains had azide bands more distant from the bulk water value (and slightly more as each polymer had a longer alkyl chain), compared to BTMA with more bulk-like water values at each % RH. Examining the data as a function of λ, as seen in Fig. 4.8 (b), shows the differences in IEC between the polymer samples.[11] In Fig 4.8 (b), all of the comb-shaped polymers at their respective λ had similar hydration of the azide, although BTMA still displayed values closer to bulk water at each λ. The observation that BTMA had more bulk-like water values at each λ (or % RH) may be indicative of higher water mobility within BTMA than within the comb-shaped polymers.

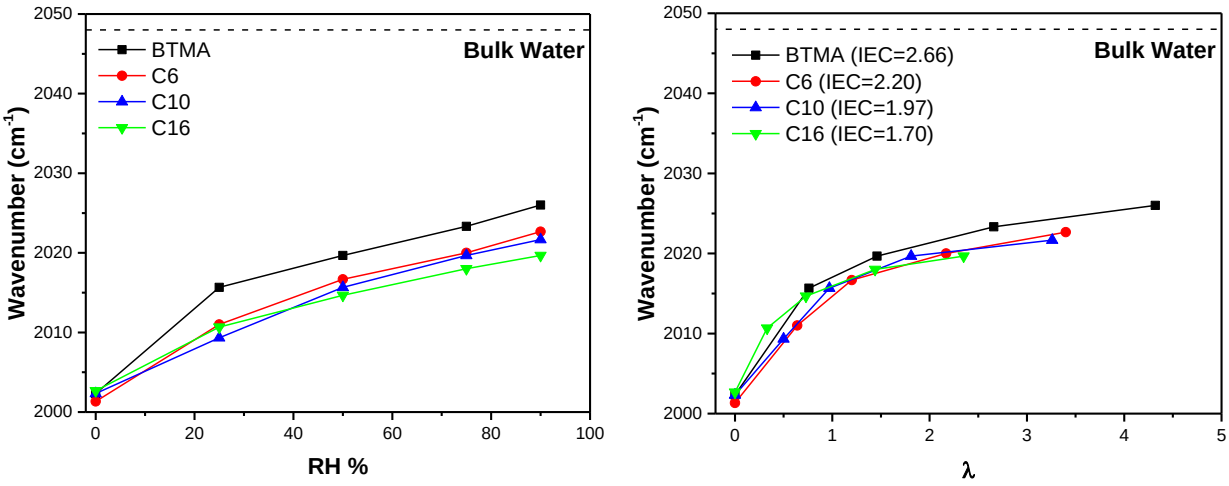

Fig. 4.8 Changes in the azide asymmetric stretch frequency for all the samples as a a) function of RH and b) function of hydration number and the dashed line represent bulk water.

The azide asymmetric stretch band spectra seen at Fig. 4.9 were all fitted for BTMA and C16 (representing the two limits) at their respective RH, and the results are depicted in Fig. 4.9. To obtain the fitting, it was first started with 0% RH. After observing

that one band did not provide an acceptable fit, a second peak was added. The bands that were fitted were then held constant with the same position and shape throughout the other RHs. An additional band was added from 25% RH, and so on, until 90% RH, to account for the azides interacting with water. These additional bands were allowed to change position and shape.

At 0% RH, findings show the presence of two bands (magenta) that represent the ”free” non-interacting azide, while the green bands represent the azide interacting with the QA component of each polymer. As RH increases, it is observed that the “free” azide (magenta) bands and the QA azide (green) bands decrease, while a new (blue) band appears. This blue band represents the azide interacting with water; so, it is designated as the “wet” band. The band positions at 0% RH are unique for each QA-PPO; these positions were held constant in the samples, and “wet” (blue) band was allowed to vary with the remaining RH values. For BTMA, at 0% RH the “free” azide (magenta) band is at ~2000 cm^{-1} and the QA azide (green) band is at ~2007 cm^{-1}, while at 90% RH, or λ=4.3, the “wet” (blue) band, i.e. where azides are forming hydrogen bonding, is at 2026 cm^{-1}. For C16, the “free” azide band is at ~1998 cm^{-1} and the QA azide band is at ~2008 cm^{-1}, while at 90% RH (or λ=2.35), the “wet” band is at ~2021 cm^{-1}.

With the dry samples (0% RH), BTMA had a slightly higher “free” azide band wavenumber than the C16; this is considered to be directly related to the fact that the QA group in BTMA is more electron deficient than the other QA-PPOs. The inductive electron-donating effect of the α carbon increases significantly when that carbon is changed from a methyl group to an ethyl group.[12] Further increases in the alkyl chain length beyond the ethyl group, have a less pronounced effect on the QA group electron

density; hence, the C16 “free” azide band has a slightly lower wavenumber. Although it is evident in BTMA that by increasing λ, the “free” azide band (magenta) promptly decreased until it disappeared; however, for C16 it required a higher hydration level (>25% RH) to eliminate the “free” azide band. The assumption for this particular finding is directly related to the presence of alkyl side chains in C16. As previously discussed, BTMA lack alkyl side chains; therefore, when water is absorbed in the membrane, the water molecules are more mobile and can access all “free” azides in the system. Because C16 contains alkyl side chains; water molecules are less mobile in the membrane, making it somewhat more difficult to promptly access all “free” azides in the system. The behavior of the “wet” azide (blue) band evidently shows, as expected, increased absorbance as λ increases, consistent with the presence of more water molecules within the polymer membrane. The green band is assumed to represent the interaction of the QA group with the azide. At λ=0, the azide is predominantly as a “free” state and interacts with the QA groups at an intermediate level; accordingly the magenta band has a slightly higher absorbance band than the green band. As λ increases, azide begins to interact with the water molecules, gradually distancing themselves from the QA groups to form a long-distance interaction; eventually, azide only interacts with water. This behavior is represented in Fig 4.9 with the gradual decrease of the green band until it disappears.

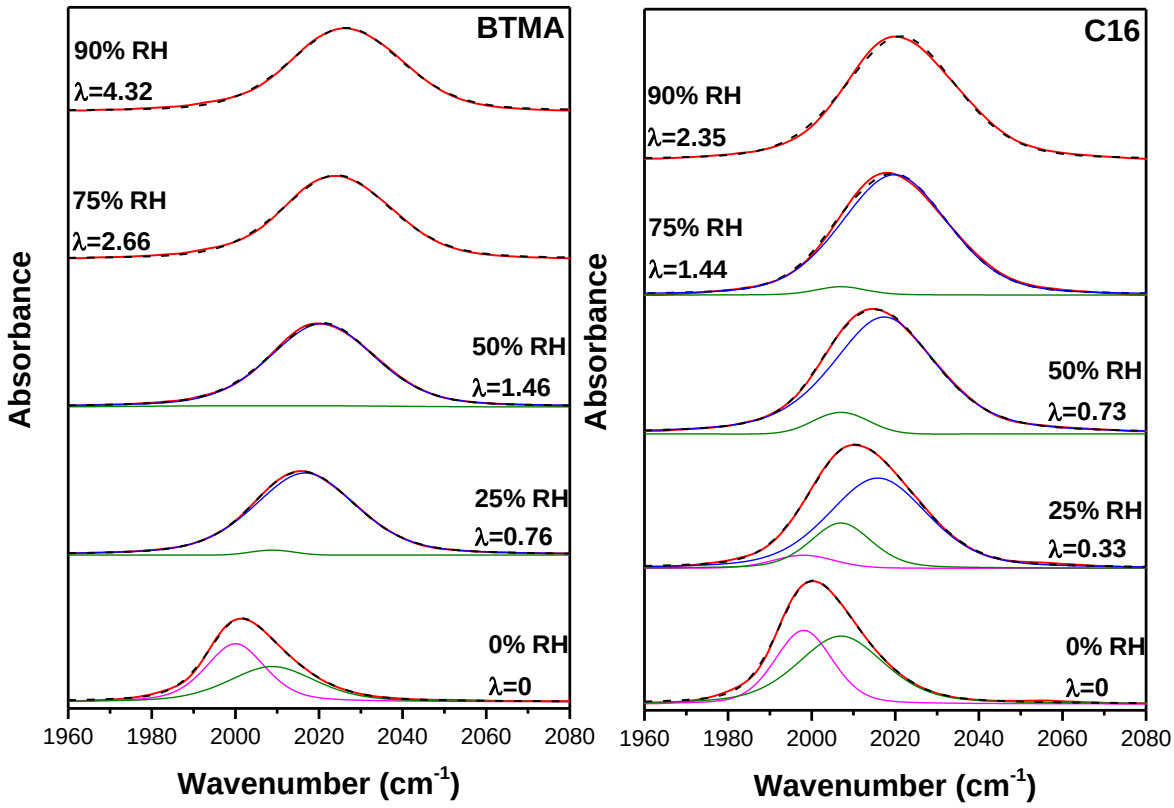

Fig. 4.9 Deconvolution of all the comb-shaped polymers in the azide asymmetric stretch using the three-population model. Where the red is the experimental spectrum and the dashed black is the fitted spectrum. "wet' band is in blue, azide interacting with the QA is in green and the "free" azides is in magenta.

4.4 Discussion on Similarities of Solutions and Polymer Studies

Our original expectation was that the dielectric constant would play a role in the peak position of the azide asymmetric stretch. However, in both the solutions and polymer studies presented here, we determined that it was the hydrogen bonding that played a dominant role in the peak position of the azide asymmetric stretch, and the role of the dielectric constant was negligible. The finding of the non-interacting azides with a peak at 2000 cm^{-1} was observed in both the polymers studies and the DMSO-water

mixtures of the solutions studies. These findings prove, furthermore, that the dielectric constant plays a negligible role on the shift of the azide asymmetric stretch.

Overall, azide is a sensitive probe that can used to characterize ion pairs and intermolecular interactions (hydrogen bonding), as seen with azide and different countercations (see Appendix D) and studies reported in literature.[5,13] Azides' capacity of detecting ion pairs became evident when the azide asymmetric stretch bands of the QA-PPO results were peak fitted and a band appeared in between the "free" azides and the "wet" band, corresponding to what is assumed to be the azide anion interacting with the cationic QA groups in the polymer system. The characterization of ion pairs also gives information of the hydrophobic components of the polymer, as seen in the results obtained on the C16.

4.4 References

(1) Sando, G. M.; Dahl, K.; Owrutsky, J. C. Vibrational Spectroscopy and Dynamics of Azide Ion in Ionic Liquid and Dimethyl Sulfoxide Water Mixtures †. **2007**, 4901–4909.

(2) Ohta, K.; Tayama, J.; Tominaga, K. Ultrafast Vibrational Dynamics of SCN− and N3− in Polar Solvents Studied by Nonlinear Infrared Spectroscopy. *Phys. Chem. Chem. Phys.* **2012**, *14* (30), 10455–10465.

(3) Li, M.; Owrutsky, J.; Sarisky, M.; Culver, J. P.; Yodh, A.; Hochstrasser, R. M. Vibrational and Rotational Relaxation Times of Solvated Molecular Ions. *J. Chem. Phys.* **1993**, *98* (7), 5499–5507.

(4) Fulmer, E. C.; Ding, F.; Zanni, M. T.; Fulmer, E. C.; Ding, F.; Zanni, M. T. Heterodyned Fifth-Order 2D-IR Spectroscopy of the Azide Ion in an Ionic Glass Heterodyned Fifth-Order 2D-IR Spectroscopy of the Azide Ion in an Ionic Glass. **2016**, *34302* (2005).

(5) Kuo, C.-H.; Vorobyev, D. Y.; Chen, J.; Hochstrasser, R. M. Correlation of the Vibrations of the Aqueous Azide Ion with the O−H Modes of Bound Water Molecules. *J. Phys. Chem. B* **2007**, *111* (50), 14028–14033.

(6) Lee, H.; Choi, J.; Cho, M. Vibrational Solvatochromism and Electrochromism of Cyanide , Thiocyanate , and Azide Anions in Water W. **2010**, 12658–12669.

(7) Ye, S.; Huber, T.; Vogel, R.; Sakmar, T. P. FTIR Analysis of GPCR Activation Using Azido Probes. *Nat. Chem. Biol.* **2009**, *5* (6), 397–399.

(8) Nydegger, M. W.; Dutta, S.; Cheatum, C. M. Two-Dimensional Infrared Study of 3-Azidopyridine as a Potential Spectroscopic Reporter of Protonation State. *J. Chem. Phys.* **2010**, *133* (13).

(9) Gai, X. S.; Coutifaris, B. A.; Brewer, S. H.; Fenlon, E. E. A Direct Comparison of Azide and Nitrile Vibrational Probes W. **2011**, 5926–5930.

(10) Son, H.; Kwon, Y.; Kim, J.; Park, S. Rotational Dynamics of Metal Azide Ion Pairs in Dimethylsulfoxide Solutions. *J. Phys. Chem. B* **2013**, *117* (9), 2748–2756.

(11) Sando, G. M.; Dahl, K.; Zhong, Q.; Owrutsky, J. C. Vibrational Relaxation of

Azide in Formamide Reverse Micelles. *J. Phys. Chem. A* **2005**, *109* (26), 5788–5792.

(12) Goutev, N.; Matsuura, H. Hydrogen Bonding in Chloroform Solutions of Ethylenedioxy Ethers. Spectroscopic Evidence of Bifurcated Hydrogen Bonds. *J. Phys. Chem. A* **2001**, *105* (19), 4741–4748.

(13) Zhong, Q.; Steinhurst, D. A.; Carpenter, E. E.; Owrutsky, J. C. Fourier Transform Infrared Spectroscopy of Azide Ion in Reverse Micelles. *Langmuir* **2002**, *18* (20), 7401–7408.

(14) Kushner, D. I.; Zhu, L.; Kusoglu, A.; Hickner, M. A. Side Chain Influence on the Mechanical Properties and Water Uptake of Confined Comb-Shaped Cationic Polymer Thin Films. *Macromol. Chem. Phys.* **2016**, n/a--n/a.

(15) Mousavi, M. P. S.; Kashefolgheta, S.; Stein, A.; Philippe, B. Electrochemical Stability of Quaternary Ammonium Cations : An Experimental and Computational Study. **2016**, *163* (2), 24–26.

Chapter 5

Conclusions and Future Work

5.1 Conclusions

The thesis work presented here was subdivided into two parts: solution studies of the azide probe and QA-PPO polymer studies. The solution studies demonstrated that hydrogen bonding played a more dominant role on the position of the azide asymmetric stretch band than the dielectric constant of the solvents. The protic solvents exhibited a blueshift to a higher wavenumber, indicative of strong interactions with the azide probe and formation of hydrogen bonds. The aprotic solvents exhibited showed a lower wavenumber, indicative of weaker interactions. However, chloroform, as a non-polar solvent, exhibiting an intermediate wavenumber (and intermediate interaction with azide), indicative of its ability to form a bifurcated hydrogen bonding, where the single hydrogen atom can participate in two hydrogen bonds. Overall, the results of these solutions studies has provided information on how azide behave in different solvent environments and, therefore, has contributed to the limited body of knowledge on the use of the azide anion as a vibrational probe.

Furthermore, the use of an azide probe to measure the hydration behavior in an AEM experimental system, such as the QA-PPO polymers, represents an innovative approach not yet reported so far, and the second part of this thesis work. The results of

the QA-PPO polymer studies demonstrated the changes in water/polymer interactions as a function of the hydration number (λ). Results indicated that the interaction of the QA-PPOs with water became stronger as the alkyl pendant of each QA-PPO was shorter. With the fitted spectral data, it was better observed at λ=0, the presence of "free" azides (~2000 cm^{-1}) and azides interacting with the QA (a weaker band at ~2008 cm^{-1}) within the polymer membranes. Data from the water/azide behavior within the QA-PPOs also revealed that a higher λ was required for the azide to fully interact with the water molecules in C16, which is the QA-PPO with the longest alkyl chains that apparently convey a more hydrophobic microenvironment.

To sum up the accomplishments, the azide was successfully employed as a vibrational probe to measure the change in water/polymer interactions and was shown to be effectively measured by ATR-FTIR. The solvent studies showed some similarities to the polymer studies and provided a fundamental basis for this work. As to the hypothesis that the spectral features of the azide probe would render information on the hydrogen bonding environment of water and different water interactions with each QA-PPO, the findings in this thesis work could only demonstrate this up to a point. Specifically, the results demonstrated how much water could the polymer absorb and the comparative hydrophobicity of the different QA-PPO polymers. Much more needs to be explored about the water interactions and the ion conductivity in AEMs, in order to fill the scientific gap and address the measures that must be taken to improve AEM technology.

5.2 Future Work

This thesis work was conducted entirely by using azide as a vibrational probe. Pursuing similar studies as presented here, but using a different probe may prove to be interesting and possibly add new information on how the anion exchange membrane (AEM) polymers interact with water. Ideally, this probe should better determine the influence of the alkyl chain length and be sensitive to the dielectric constant of the polymer membranes. Unfortunately, this alternative probe has yet to be identified. Within this thesis discussion, it was presented that the azide anion forms a covalent bond with the polymer, which then causes its degradation (see Appendix C), but this is an area that still requires further research.

Another aspect worth mentioning is the fact that this work was only performed with AEM polymers. Similar work on PEM polymers, using an azide probe, might be interesting and may add more information to the already extensive body of studies done with PEM polymers, such as Nafion® for example. The OD stretch has been widely used to study hydration in PEMs, even with newly presented polymers; however, studying hydration in PEMs with the use of azide can elicit results that can be readily compared with the OD stretch to see if the peak fitting done with the azide gives similar findings to the peak fitting done with the OD stretch.

Appendix A: Contact Ion Pairs observed in Sodium Azide

The Fig. A.1 demonstrates the FTIR spectra of different solvents with NaN_3 and with $TBAN_3$. Fig. A.1 (a) shows NaN_3 with several solutions and the relationship between the wavenumber position and the nature of the solvent. Specifically, the solvents were water, DMSO, methanol (MeOH) and dimethylformamide (DMF). Secondary shoulder peaks were observed with the aprotic solvents (DMF and DMSO) and were attributed to the formation of ion pairs between the azide anion and the partially solvated counterion. Taking water as an example, the Na^+ ion is completely solvated in water and more distant from the N_3^- ion to be able to interact and form a contact pair; thus, only a single azide asymmetric stretch peak is observed at 2048 cm^{-1} (without a shoulder). In contrast, in DMSO the Na^+ ion is not fully solvated; so, a solvent separated azide asymmetric stretch band appears at 2000 cm^{-1} and a contact ion pair peak appears at 2022 cm^{-1} due to the interaction of the counterion with the azide.

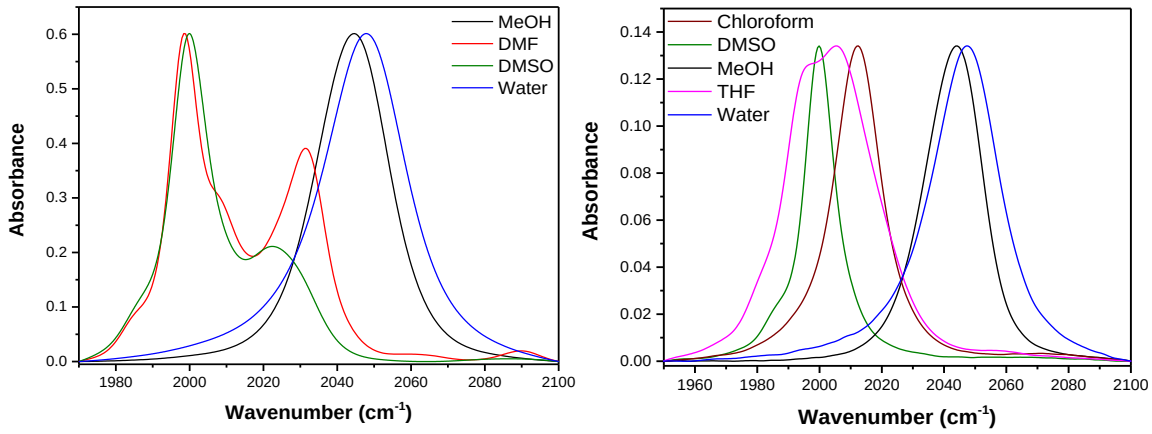

Fig. A.1 FTIR spectra of different solvents in (a) 0.26M NaN_3 and (b) 0.05M $TBAN_3$.

The complication of the azide spectra introduced by the formation of ion pairs can be eliminated by selecting a counterion that readily interacts with the solvent and does not form a contact pair with the azide. This is the main reason why $TBAN_3$ was selected to conduct further studies. Having no ion-pair band, it simplifies the spectral fitting, as shown in Fig. 4.5 (b), and the effects of the counterion on the N_3^- ion do not have to be considered in order to interpret the behavior of peaks. Curiously, when comparing the peak positions with the protic solvents, slight differences were found. For example, in water NaN_3 showed a peak position at 2048 cm^{-1}, while with $TBAN_3$ the peak position was at 2047 cm^{-1}; in methanol NaN_3 had a peak position at 2045 cm^{-1}, while with $TBAN_3$ the peak position was at 2043 cm^{-1}. The finding of a slightly lower wavenumber for $TBAN_3$ in comparison to NaN_3, can be explained because the major component (TBA) has both hydrophilic and hydrophobic domains, and the hydrophobic domains (found in the alkyl chains in the TBA) does not allow it to reach the same wavenumber as NaN_3.

Appendix B: Parameters Determined from the Azide Band in the Four Sets of Mixtures

Table B0.1 Parameters determined from Azide band in DMSO-Water mixtures

Mole Fraction	"Hot" band				"Dry" band				"Wet" band			
	Wavenumber (cm^{-1})	Width (cm^{-1})	Intensity	Fraction Lorentzian	Wavenumber (cm^{-1})	Width (cm^{-1})	Intensity	Fraction Lorentzian	Wavenumber (cm^{-1})	Width (cm^{-1})	Intensity	Fraction Lorentzian
0	1985.10	6.04	0.01	0	2000.04	11.65	0.13	0.89				
0.02	1987.35	9.23	0.02	1.00	1999.89	10.49	0.11	0.20	2009.22	13.89	0.05	1.00
0.06	1988.90	8.27	0.01	0	1999.53	9.59	0.05	0	2009.37	18.40	0.13	0.75
0.10	1986.70	8.82	0.01	0	1999.35	10.27	0.03	0.23	2009.82	19.91	0.13	0.53
0.15	1987.43	22.45	0.01	1.00	1998.40	5.29	0.01	0	2010.47	22.45	0.13	0.17
0.25									2011.22	24.21	0.13	0.22
0.50									2021.45	24.10	0.13	0.36
0.75									2032.90	24.11	0.13	0.38
0.90									2040.90	24.96	0.13	0.52
1									2046.80	25.64	0.13	0.59

Table B0.2 Parameters determined from Azide band in THF-Water mixtures

Mole Fraction	Unknown band				Dry band				Solution band			
	Wavenumber (cm^{-1})	Width (cm^{-1})	Intensity	Fraction Lorentzian	Wavenumber (cm^{-1})	Width (cm^{-1})	Intensity	Fraction Lorentzian	Wavenumber (cm^{-1})	Width (cm^{-1})	Intensity	Fraction Lorentzian
0	1993.28	7.83	0.02	0	2004.51	31.05	0.13	0.28				
0.02					2018.00	26.59	0.08	0	2027.18	19.82	0.06	0.58
0.06									2027.38	30.192	0.13	0.35
0.10									2027.83	29.73	0.13	0.34
0.15									2028.49	29.37	0.13	0.34
0.25									2028.66	29.70	0.13	0.35
0.50									2033.79	28.28	0.13	0.40
0.75									2038.11	27.35	0.13	0.43
0.90									2042.43	26.29	0.13	0.49
1									2046.80	25.63	0.13	0.60

Table B0.3 Parameters determined from Azide band in Chloroform-MeOH mixtures

Mole Fraction	Solution band			
	Wavenumber (cm^{-1})	Width (cm^{-1})	Intensity	Fraction Lorentzian
0	2012.14	17.87	0.12	0.73
0.02	2023.86	25.93	0.12	0.33
0.06	2027.61	25.96	0.12	0.32
0.10	2030.07	25.88	0.12	0.31
0.15	2032.05	25.43	0.12	0.29
0.25	2034.53	25.20	0.12	0.26
0.50	2037.26	24.43	0.12	0.24
0.75	2040.44	23.25	0.12	0.24
0.90	2041.72	22.49	0.12	0.25
1	2043.03	21.72	0.12	0.30

Table B0.4 Parameters determined from Azide band in DMSO - Chloroform mixtures

Mole Fraction	Azide band				Hot band band			
	Wavenumber (cm^{-1})	Width (cm^{-1})	Intensity	Fraction Lorentzian	Wavenumber (cm^{-1})	Width (cm^{-1})	Intensity	Fraction Lorentzian
0	2000.04	1.64	0.13	0.81	1985.23	6.56	0.01	0
0.02	2001.58	4.82	0.13	0.69	1984.87	5.24	0.01	0
0.06	2001.85	5.21	0.13	0.64	1985.80	5.21	0.01	0
0.10	2002.06	5.25	0.13	0.50	1984.81	7.57	0.01	0
0.15	2003.63	7.05	0.13	0.57	1985.10	3.00	0.01	0
0.25	2003.76	6.78	0.13	0.43	1985.06	8.42	0.01	0
0.50	2007.901	7.26	0.13	0.47				
0.75	2010.53	6.56	0.13	0.49				
0.90	2011.20	6.31	0.13	0.49				
1	2012.192	7.63	0.13	0.49				

Appendix C: QA-PPO in Azide Form

Throughout the studies presented thus far, the QA-PPO polymers were in their bromide form and the inserted azide ions did not disturb the polymer membrane. Deciding to further the investigation here, we decided to make a complete ion exchange of the Br^- to the N_3^- by soaking the polymer membrane in 1M NaN_3 for approximately 24 hours. After the film was recasted on the Ge crystal and studied by FTIR, the results are shown in Fig. 4.9. To our surprise, the υ_3 stretch peak is no longer at 2000 cm^{-1}; they all blueshifted, but slightly more as each polymer had a longer alkyl chain. A new peak appeared at 2101 cm^{-1}, which we first assumed it was the NR_4^+ N_3^- contact pair. However, in a study of ionic salts catalyzing the coupling reaction between epoxide and carbon dioxide by Foltran, et al[1], they observed another band at about 2100 cm^{-1}. The researchers concluded that this 2100 cm^{-1} band corresponded to the asymmetric stretching vibration υ(C-N) of an intermediate component, resulting from the attack of the azide ion onto the epoxide ring leading to the formation of an "organic azide". The researchers described the organic azide to be very stable and its behavior displayed the "poor-leaving" ability of azides.[2]

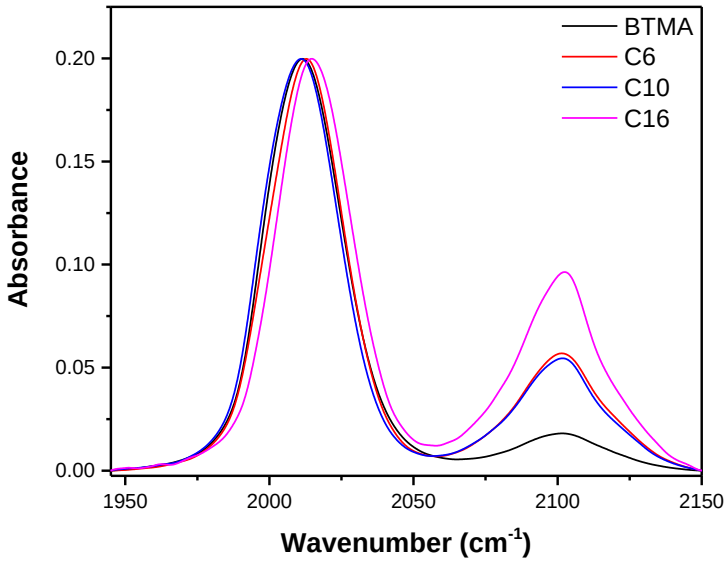

Fig. C.1 Overlaid spectra of all the dry QA-PPO samples in azide form to show spectral differences in the azide peak and additional peak formation (~2100 cm^{-1}) relative to the change in the alkyl chain lengths.

We decided to test for the formation of a covalent bond with the alkyl chain, as described in the Foltron study[14]. A membrane of C10 in azide form was casted, and then was ion exchanged back to the Br^- form by soaking the polymer membrane in 1M NaBr for approximately 24 hours. After the soak, it was casted in a Ge crystal and studied by FTIR, and the results are shown in Fig 4.10. When the QA-PPO was changed back to the Br^- form, it no longer exhibited a peak at 2000 cm^{-1}; so, no free N_3^- ions were present. Yet the 2101 cm^{-1} band persisted, indicating the formation of something different from the original polymers. This by-product was no longer soluble in methanol, as the original polymer, precluding the ability to study it further in the H^1 NMR. More studies are required to better understand this phenomenon; but for now, we assume that with the longer soaking time the polymer experienced some form of degradation.

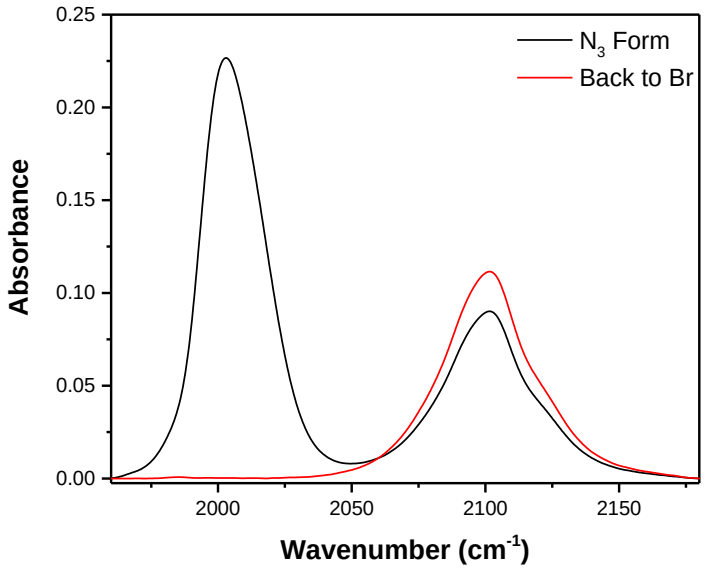

Fig. C.2 Spectra of the QA-PPO C10 in dry azide form (black) and the C10 changed back into the Br^- form (red). The additional peak (~2100 cm^{-1}) was still present even though there were no free N_3^-.

References:

(1) Foltran, S.; Alsarraf, J.; Robert, F.; Landais, Y.; Cloutet, E.; Cramail, H.; Tassaing, T. On the Chemical Fixation of Supercritical Carbon Dioxide with Epoxides Catalyzed by Ionic Salts: An in Situ FTIR and Raman Study. *Catal. Sci. Technol. Catal. Sci. Technol* **2013**, *3* (3), 1046–1055.

(2) Kiasat, A. R.; Badri, R.; Zargar, B.; Sayyahi, S. Poly (Ethylene Glycol) Grafted onto Dowex Resin : An Efficient , Recyclable , and Mild Polymer-Supported Phase Transfer Catalyst for the Regioselective Azidolysis of Epoxides in Water. **2008**, No. 7, 8382–8385.

Appendix D: Azide and Different Countercations

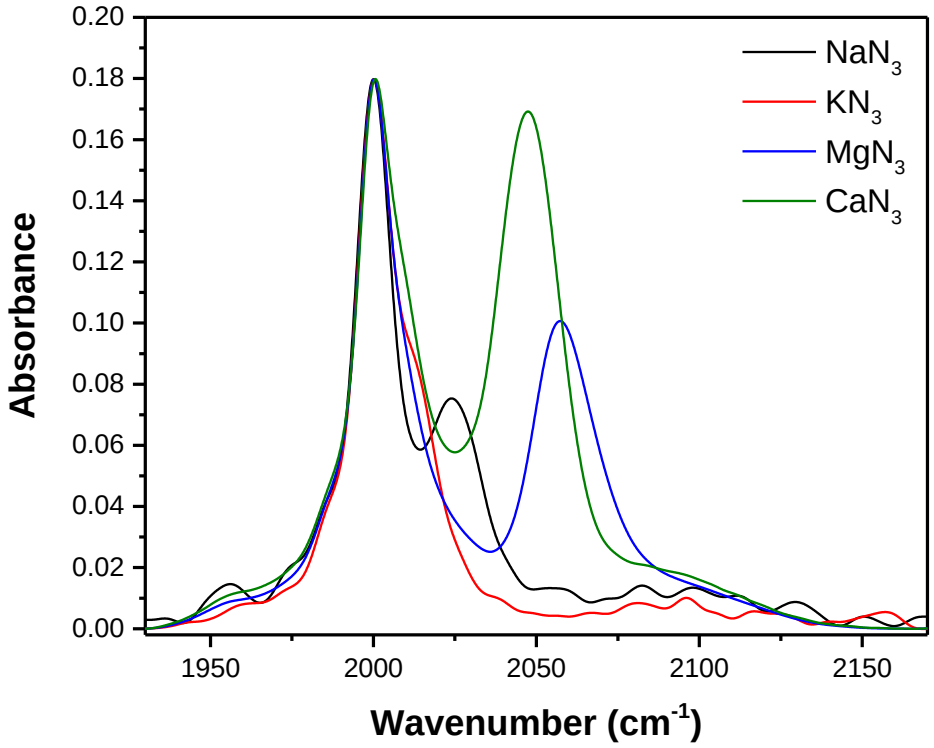

Fig. D.1 FTIR spectra of the asymmetric stretching mode of azide in DMSO. The peak at 2000 cm^{-1} results from the "free" azide, while the peaks at higher frequency is from the ion pairs. The ion pairs were blueshifted in accordance to the countercations.